IOWA STATE UNIVERSITY
Digital Repository

Graduate Theses and Dissertations

Iowa State University Capstones, Theses and Dissertations

2010

A comparison study of digital sinusoidal fringe generation technique: defocusing binary patterns VS focusing sinusoidal patterns

Shuangyan Lei
Iowa State University

Follow this and additional works at: https://lib.dr.iastate.edu/etd

 Part of the Mechanical Engineering Commons

Recommended Citation
Lei, Shuangyan, "A comparison study of digital sinusoidal fringe generation technique: defocusing binary patterns VS focusing sinusoidal patterns" (2010). *Graduate Theses and Dissertations*. 11740.
https://lib.dr.iastate.edu/etd/11740

This Thesis is brought to you for free and open access by the Iowa State University Capstones, Theses and Dissertations at Iowa State University Digital Repository. It has been accepted for inclusion in Graduate Theses and Dissertations by an authorized administrator of Iowa State University Digital Repository. For more information, please contact digirep@iastate.edu.

www.manaraa.com

A comparison study of digital sinusoidal fringe generation technique: defocusing binary patterns VS focusing sinusoidal patterns

by

Shuangyan Lei

A thesis submitted to the graduate faculty

in partial fulfillment of the requirements for the degree of

MASTER OF SCIENCE

Major: Mechanical Engineering

Program of Study Committee:
Song Zhang, Major Professor
James Oliver
Eliot Winer
Lie Tang

Iowa State University

Ames, Iowa

2010

www.manaraa.com

TABLE OF CONTENTS

www.manaraa.com

www.manaraa.com

LIST OF FIGURES

www.manaraa.com

www.manaraa.com

www.manaraa.com

ABSTRACT

With the recent advancements in digital technology, three-dimensional (3-D) shape measurement has played an increasingly important role in fields including manufacturing, homeland security, medical sciences, and entertainment. Over the past decades, numerous 3-D shape measurement techniques have been developed. Among these existing techniques, fringe analysis based on phase-shifting sinusoidal structured patterns stands out because of its numerous advantages. However, there are still some major challenges of the existing digital fringe projection system for accurate 3-D shape measurement and for future speed improvement. They are: (1) projector nonlinearity problem, (2) synchronization problem, and (3) exposure time limitation problem. There are currently two approaches to generate sinusoidal fringe patterns with a digital-light-processing (DLP) projector: defocusing binary patterns (DBP) and focusing sinusoidal patterns (FSP). The focus of this dissertation research is to compare these methods for high-quality 3-D shape measurement.

We developed a system based on a digital fringe projection and phase-shifting technique to perform various comparison tests. The system utilizes a DLP projector to project computer generated fringe patterns onto the object and a charged-coupled-device (CCD) camera to acquire the fringe images. Conventionally, sinusoidal fringe patterns are usually supplied to a focused projector, and the DBP method is used to properly defocus the projector to generate sinusoidal patterns from binary structured patterns. We compare the performance of the new DBP approach against the traditional FSP method by analyzing the phase errors introduced by following factors: (1) defocusing degree, (2) exposure time, (3) synchronization, and (4) projector nonlinear gamma.

www.manaraa.com

The traditional FSP involves some practical issues for high-quality measurement. Our experiment found it is possible to generate ideal sinusoidal fringe patterns by the DBP method, and when the projector is defocused to a certain degree, the phase error induced by the DBP method is very close to that produced by the FSP approach. With the DBP method, 3-D reconstruction was shown to be feasible.

Short exposure time is especially needed when measuring fast motion. For the FSP method, the minimum exposure time of the camera is limited by the projector's fringe projection rate, and the phase error is very large when a very short exposure time is needed. The experimental results show that the phase error does not change very much when the exposure time alters, and if a very short exposure time is needed, the DBP method clearly outperforms the FSP method for 3-D shape measurement. It also provides a potential way to develop fast 3-D shape measurement technique.

For the DLP projector, if it is supplied with sinusoidal fringe patterns, the synchronization between the projector and the camera is critical. When the projector is not synchronized with the camera, the phase error for the DBP method is much smaller than that for the FSP method when the exposure time is not multiples of projection cycle. By implementing the DBP method in our system, we could achieve 3-D reconstruction without synchronization between the projector and the camera.

Projector gamma correction, which is usually a time-consuming procedure, is mandatory for the FSP method. In this research, we found no projector gamma correction is needed for the DBP method. Our experimental results demonstrated it can achieve high-quality 3-D reconstruction by the DBP method without projector nonlinearity calibration.

www.manaraa.com

Compared with the FSP method, the possible shortcomings of the DBP method are: (1) seemingly sinusoidal fringe patterns are still composed of high-frequency harmonics, which results in measurement error, and (2) the depth range of high-contrast fringe patterns is small. Even with these drawbacks, this new technique still has the potential to replace the conventional fringe generation technique.

www.manaraa.com

CHAPTER 1. INTRODUCTION

With the recent advancements in digital technology, the use of fringe projection techniques for 3-D shape measurement techniques has become one of the most active research areas in optical metrology [1]. Among the various fringe analysis techniques, the one employing sinusoidal fringe patterns and phase shifting approach is one of the most widely used due to its speed and accuracy [2]. However, there are some practical issues to be considered for high quality measurement and for its speed improvement. Currently, there are two approaches to generate sinusoidal fringe patterns with a DLP projector: DBP and FSP. The objective of this dissertation research is to compare these methods with respect to the following issues: (1) degree of defocusing, (2) exposure time, (3) synchronization, and (4) projector nonlinear gamma. Studying how to use a commercial projector to realize real-time, low-cost, reliable, and accurate 3-D shape measurement is highly needed.

State of the art is reviewed in Section 1.1. The motivations of this research are introduced in Section 1.2. The objective of this research is addressed in Section 1.3, and Section 1.4 presents the organization of this dissertation.

1.1 State of the art

3-D shape measurement technique is concerned with extracting the depth information from the image of the measured object. The methods investigating this topic fall into two categories, passive and active, depending on their source to sense the object [3].

The passive methods are essentially to capture photographs of the object from different viewing angles, and to obtain the depth information by finding the correspondence

www.manaraa.com

between images and establishing the triangulation relationship between the object point and the camera sensors. Active methods, on the other hand, recover depth information by actively putting some pre-defined structured patterns onto the object surface to assist the corresponding identifications. Our work falls in the category of the active methods.

The structured light is defined as the projection of simple or encoded light patterns (i.e. points, lines, grids, complex shapes) onto the illuminated scene [4]. Due to its merits of easy implement and fast full field measurement, the structured light method has been widely used in the field of vision-based, non-contact 3-D shape measurement [5].

Zhang & Huang put forward a technique called digital fringe projection and phase-shifting technique and have successfully developed a high-resolution, real-time 3-D shape measurement system, which achieved simultaneous 3-D shape acquisition, reconstruction, and display at a speed of 40 frame/sec [6]. Chen et al. presented an idea of designing uniquely color-encoded pattern projection to realize 3-D shape reconstruction with only local analysis of a single image. The system has the advantage of dynamically adjusting the position between the camera and the projector [7]. Based on the combination of gray-coded and phase-shifting methods, Chen et al. developed an accurate 3-D shape measurement system to reach 360^{o} measurement. The average standard deviation is 0.076 mm for a plaster model with the volume of 320 mm × 200 mm × 250 mm [8]. All of those techniques require structured light patterns are sent to a focused projector to fulfill precise 3-D shape measurement, which belongs to the FSP approach.

Shape recovery from the defocusing method is different from that of the focus method. It needs to compute the blur degree of the images and carefully calibrate the imaging system about its blurring characteristics [9]. Without precisely estimating the defocusing

www.manaraa.com

blur, it would not be possible to obtain the proper reconstruction. Hinojosa et al. developed a 3-D shape measurement system by using projections of cylindrical wavefronts on the object to extract the depth information of the objects from the defocusing structured light (DSL) image and recover the 3-D surface information [10]. However, this approach has not realized real-time 3-D shape measurement.

A fringe pattern is essentially a special case of structured light pattern in which the stripe intensity varies sinusoidally. Conventionally, the fringe patterns are generated either by a mechanical grating or by laser interference. With recent advancements in digital display technology, which has the advantage of generating and controlling the fringe patterns accurately and easily, 3-D shape measurement based on the fringe projection techniques has become one of the most brisk fields in optical metrology and has various applications in diverse fields [11-14].

Although the traditional FSP approach based on digital fringe projection and phase-shifting technique has been widely adopted, there are practical considerations of the existing digital fringe projection technique:

(1) **Projector nonlinearity problem**. Because the commercial video projector is usually a nonlinear device that is purposely designed to compensate for human vision, generation of sinusoidal fringe image is difficult. Therefore, to perform high quality 3-D shape measurement using a digital fringe projection and phase-shifting method, the projector nonlinearity calibration is usually mandatory. Different methods have been developed to calibrate and correct the nonlinearity of the projector [15-20]. The projector nonlinearity calibration increases the complexity of the system development. Moreover, our experiments found that the

www.manaraa.com

projector nonlinearity changes overtime, thus it needs to be re-calibrated frequently for high quality measurement.

(2) **Synchronization problem**. Because the DLP projector generates one full grayscale image by time modulation [21], it is vital to capture the whole channel projection in order to acquire correct and accurate grayscale images. Therefore, if sinusoidal fringe patterns are supplied to the projector, the synchronization between the projector and the camera is critical and the exposure time of the camera must be precisely controlled. This means that the camera must start its exposure when the image starts refresh, and must stop its exposure when it finishes refresh.

(3) **Exposure time limitation problem**. Since the projector and the camera must be precisely synchronized, the minimum exposure time of the camera is limited by the projector's fringe projection rate, typical 120 HZ for a DLP projector. The camera exposure time cannot be shorter than the single channel projection time 2.78 ms (1/360 sec). This certainly limits its application to measure fast motion when a very short exposure time is needed.

To avoid these problems, one approach is to use the DLP Discovery platform developed by Texas Instruments (TI). With DLP Discovery board, high-speed, highly linear sinusoidal fringe patterns can be generated, and the synchronization between the camera and the projector can be precisely controlled [22, 23]. However, compared with a commercial DLP projector, the DLP Discovery platform is much more expensive. Therefore, studying how to use a commercial projector to realize real-time, low-cost, reliable, and accurate 3-D shape measurement is highly needed. Although the existing technology does still not reach

www.manaraa.com

all these features together, in this dissertation, we will present a DBP approach and give a comparison study of digital sinusoidal fringe generation technique, and the research work in this thesis will bring a new perspective to the goal.

The idea of generating sinusoidal fringe patterns by the DBP method comes from our two observations [24]: (1) seemingly sinusoidal fringe patterns often appear on the ground when the light shines through open window blinds, and (2) the sharp features of an object are blended together in a blurring image that is captured by an out-of-focus camera. The former gives the insight that an ideal sinusoidal fringe image could be produced from a binary structured pattern, and the latter provides the hint that if the projector is defocused, the binary structured pattern might become an idea sinusoidal one.

The DBP approach takes the advantage of the operation principle of an optical switch called digital micromirror device (DMD) in a DLP projector [21, 25]. DMD consists of an array of tiny mirrors, and each mirror can reflect light in one of two directions, depending on the state of the underlying memory. When the memory state is in the ON state (1), the mirror tilts $+\theta$ degrees as to reflect light towards the projection aperture. When the memory state is in the OFF state (0), the mirror tilts $-\theta$ degrees as to reflect light towards the projector aperture, as seen in Figure 1. Thus, the ON state of the mirror appears bright and the OFF state of the mirror appears dark, and the grayscale values of the image are generated by controlling the percentage of ON time of the micromirror during one frame period. For instance, when a uniform image with grayscale values of 255 is supplied to a DLP projector, the micromirrors have the duty cycle of almost 100% ON. If the grayscale value is reduced to 128, each micromirror stays ON for only half of the projection cycle time. When the input gray scale is reduced to 64, the time that each micromirror stays ON is 1/4 projection cycle.

www.manaraa.com

Figure 2 shows the schematic diagram of a single-chip DLP projector. The white light first generated by the lamp in a DLP projection system passes through a color wheel filter as it travels to the DMD chip. The color wheel composed of RGB color filter spins at a high speed producing red, green, and blue light sequentially that illuminates the DMD surface. The DMD synchronizes with the color light, reflects it based on the color shining on it and forms three color channel images. By this way, the color channel images are outputted sequentially onto the screen. Due to its high resolution, high optical efficiency and brightness,

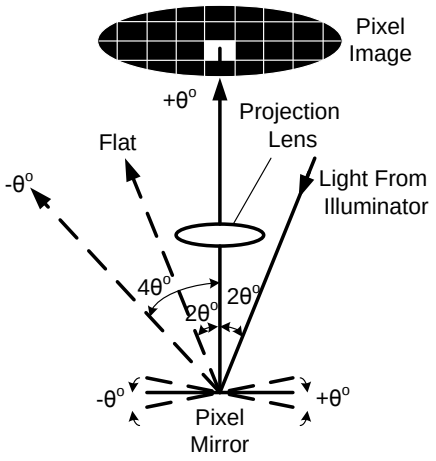

Figure 1. DMD optical switching principle [21].

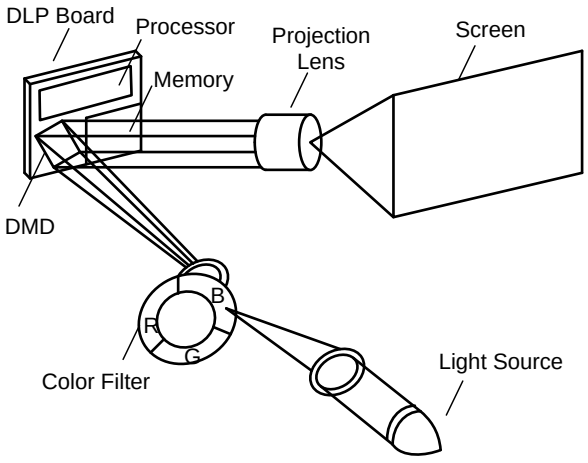

Figure 2. Schematic diagram of a single chip DLP projector [21].

www.manaraa.com

high speed, and robust stability [21], the DLP display supersedes with Cathode Ray Tube (CRT) or Liquid Crystal Display (LCD) displays and becomes one of the most active applications in digital fringe generation technique.

For the DBP approach, the computer generates gray scale images with binary state (0 or 255) are used, which means each micromirror is always set to be a value of 0 or 255, it should stay OFF or ON all the time. By this means, the micromirror will act as "solid state" (does not flash) [26]. Therefore, the fringe patterns are always generated in solid state and any segment of time can represent the produced signal, which means no precise synchronization between the projector and the camera is needed. At the same time, the exposure time of the camera can be shorter than one projection cycle. With this new technology, the 3-D shape system can measure fast motion and the measurement speed could be greatly improved. Thus, the DBP method clearly has the potential to develop high-speed real-time 3-D shape measurement.

The major contribution of this research is that it does a comparison study of sinusoidal fringe generation techniques between the DBP method and the traditional FSP approach. The experimental results have verified that generating sinusoidal fringe images by the DBP is less sensitive to the exposure time used, to the synchronization between the projector and the camera, and to the projector nonlinear gamma. On the contrast, for the conventional FSP method, all these factors must be well controlled to ensure high-quality 3-D measurement. Thus, this DBP technique can be used to measure fast motion when a very short exposure time is needed and has significantly simplified the development of 3-D shape measurement system. Compared with the FSP method, the DBP technique has the potential

www.manaraa.com

to replace the conventional fringe generation technique for 3-D shape measurement based on fringe analysis techniques.

1.2 Motivation

Over the past years, a number of 3-D shape measurement techniques have been developed including some with real-time capabilities [27-31]. 3-D shape measurement using a DLP projector becomes increasingly popular during the past few years. Among these existing 3-D shape measurement techniques, the use of fringe projection techniques for generating 3-D surface information has become one of the most popular research areas in optical metrology because of its ability to provide high-resolution, whole-field 3-D reconstruction of objects in a non-contact manner at high speed [1].

Although the conventional FSP approach based on a digital fringe projection and phase-shifting technique has been widely adopted, there are three major problems for accurate 3-D shape measurement and for future speed improvement: (1) projection nonlinearity problem, (2) synchronization problem, and (3) exposure time limitation problem. Our recent study has found that using a DBP approach can simplify or alleviate these problems relating to the ideal fringe generations with a digital video projector [24, 32]. In this dissertation, we will have a comparison study about these two methods for high-quality 3-D shape measurement.

1.3 Objective

The aim of this research is to compare the DBP method and the FSP method with respect to the following factors: (1) degree of defocusing, (2) exposure time, (3)

www.manaraa.com

synchronization, and (4) projector nonlinear gamma. In this dissertation, the fundamentals of these two techniques will be explained, the defocusing simulation for the DBP method and the experimental results for the comparison study will be shown, and the advantages and disadvantages of the DBP method compared to the FSP method will be discussed.

1.4 Organization of this dissertation

This dissertation is organized as follows: Chapter 1 discusses the motivation of using defocusing binary pattern method for the 3-D shape measurement. Chapter 2 describes the methodology and explains the details of the technique. Chapter 3 contains the theoretical background related to optics. Chapter 4 shows some simulation results. Chapter 5 presents experimental results and discusses these two approaches. Chapter 6 summarizes this thesis and discusses some future work.

www.manaraa.com

CHAPTER 2. METHODOLOGY

To realize pixel-level spatial resolution, sinusoidal fringe patterns are preferable. Conventionally, the sinusoidal fringe patterns are generated by laser interference. This has been widely adopted in optical metrology. However, because there are some problems related to coherent light, such as speckle noise, white light-based techniques have been extensively used. With the advancements of digital display technology, fringe projection based methods have been increasingly studied in recent years. In this section, we will address the physics background of sinusoidal fringe generation techniques, and then focus on digital fringe projection techniques.

2.1 Sinusoidal fringe generation

Traditionally, phase shifted sinusoidal fringe patterns are generated by interfering a time-varying phase-shifted reference wavefront with the test wavefront. At each measurement point, a time varying signal is produced, and then the relative phase between the two wavefronts at that point is encoded in these signals.

From physical optics, the wavefront of a light source is:

$$w(x, y, z) = a(x, y)e^{i\phi(x,y)} \quad (1)$$

Where x and y are spatial coordinates, and $a(x,y)$ is the wavefront amplitude. The wavefront phase can be written as:

$$\phi(x, y) = 4\pi h(x, y) / \lambda \quad (2)$$

Here, λ is the wavelength, and $h(x,y)$ is the surface height under test. The equations for the reference and test wavafronts in the interferometer are: $w_r(x, y, t) = a_r(x, y)e^{i\phi_r(x,y)-\delta(t)}$ and

www.manaraa.com

$w_t(x,y,t) = a_t(x,y)e^{i\phi_t(x,y)-\delta(t)}$, respectively, where $a_r(x,y)$ and $a_t(x,y)$ are the wavefront amplitudes, $\phi_r(x,y)$ and $\phi_t(x,y)$ are the wavefront phases, and $\delta(x,y)$ is the time-varying phase shift. When the reference and test wavefront interfere with each other, its intensity will be:

$$I(x,y,t) = |w_r(x,y,t) + w_t(x,y,t)|^2 , \tag{3}$$

Or

$$I(x,y,t) = I'(x,y) + I''(x,y)\cos[\phi_t(x,y) - \phi_r(x,y) + \delta(t)] . \tag{4}$$

Where $I'(x,y) = a_r^2(x,y) + a_t^2(x,y)$ and $I''(x,y) = 2a_r(x,y)a_t(x,y)$ are the average intensity and the intensity modulation, respectively. If we define the phase difference as $\phi(x,y) = \phi_t(x,y) - \phi_r(x,y)$, the resultant intensity image is:

$$I(x,y,t) = I'(x,y) + I''(x,y)\cos[\phi(x,y) + \delta(t)] . \tag{5}$$

Where $\phi(x,y)$ is the unknown phase related to the temporal phase shift of the sinusoidal variation. By computing the temporal delay at all the required measurement points, the whole map of the unknown wavefront $\phi(x,y)$ can be obtained.

2.2 Three-step phase-shifting algorithm

Optical metrology using fringe analysis is widely used in numerous applications because of its measurement accuracy and non-contact surface measurement nature. In order to perform a measurement, the phase needs to be retrieved from the fringe images. Generally, more fringe images that are used, the better the measurement that can be obtained. However, taking more fringe images will reduce the measurement speed. From Equation (5), we know

www.manaraa.com

that at least three fringe images with known phase shift are required to uniquely solve for the phase. In this research, we use a three-step phase-shifting algorithm with a phase shift of 2π/3, and the intensities of the three phase-shifted fringe images are:

$$I_1(x,y) = I'(x,y) + I''(x,y)\cos[\phi(x,y) - 2\pi/3], \tag{6}$$

$$I_2(x,y) = I'(x,y) + I''(x,y)\cos[\phi(x,y)], \tag{7}$$

$$I_3(x,y) = I'(x,y) + I''(x,y)\cos[\phi(x,y) + 2\pi/3]\ . \tag{8}$$

Where $I'(x,y)$ is the average intensity, $I''(x,y)$ is the intensity modulation, and $\phi(x,y)$ is the phase to be solved for. Solving Equations (6)-(8) simultaneously, we obtain the phase,

$$\phi(x,y) = \tan^{-1}\left[\frac{\sqrt{3}(I_1 - I_3)}{2I_2 - I_1 - I_3}\right], \tag{9}$$

and the data modulation,

$$\gamma(x,y) = \frac{I''}{I'} = \frac{\sqrt{3(I_1 - I_3)^2 + (2I_2 - I_1 - I_3)^2}}{I_1 + I_2 + I_3}\ . \tag{10}$$

The Equation (9) indicates that the phase value obtained ranges from – π to + π. To obtain a continuous phase map, a phase unwrapping algorithm is applied to detect the 2π discontinuities and remove them by adding or subtracting multiples of 2π [33]. Data modulation, $\gamma(x,y)$, has a value between 0 and 1, and can be used to determine the quality of the data point with 1 being the best.

2.3 Digital fringe projection and phase shifting method

Conventionally, the fringe images are generated by laser interference, which gives good precision. However, the problem of using laser is that the speckle noise is very difficult

www.manaraa.com

to remove, and the precise phase shift is hard to achieve. In this section, we will introduce a digital fringe projection and phase shifting method.

Digital fringe projection is a technique that takes advantages of the digital video projection technology. Instead of using laser interference, it uses a computer to generate fringe patterns. Figure 3 shows the typical setup of a digital fringe projection system. A projector projects vertically or horizontally straight fringe stripes onto the object. The fringe patterns will change from straight stripes to curved ones due to the object's surface geometry. A camera captures these reflected fringe patterns, which will be analyzed by the computer software. If the correspondence between the camera and the projector is known, 3-D information can be obtained through triangulation ($\triangle ABC$).

Compared with laser interference based technology, the major advantages of using a digital fringe projection technique are [34]: (1) no speckle noise. Instead of using a coherent light source, white light can be used for this technology. Therefore, the problems induced by coherent light source do not exist; (2) the profile of the patterns can be accurately controlled by software; and (3) the phase shift error caused by mechanical devices (e.g. pizeo) for phase shifting is eliminated because the phase shift is generated digitally.

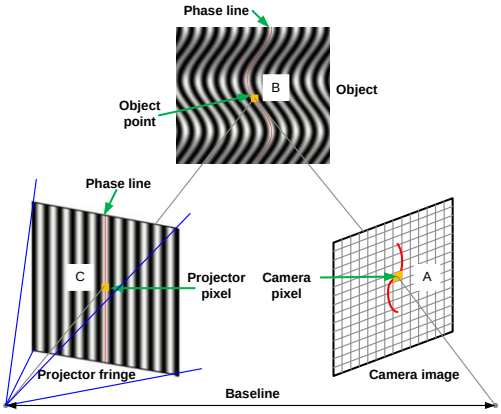

Figure 3. Typical setup of a digital fringe projection and phase shifting system.

www.manaraa.com

2.4 Projector nonlinearity correction

However, the traditional fringe projection technique is not trouble free. One of the major problems is the projector nonlinear gamma response. This is because the commercial video projector is usually a nonlinear device that is purposely designed to compensate for human vision. This nonlinear response will result in non-sinusoidal waveforms if no compensation is used. For the digital fringe projection and phase-shifting method, the non-sinusoidal waveforms are the primary source of error because the phase shift error is not present due to its digital fringe generation nature. Over the years, various nonlinear gamma correction methods have been proposed. In general, they can be classified into two categories, active methods, and passive methods. The active methods essentially pre-deform the waveform of the fringe patterns generated by the computer before sending to the computer [15,16] while the passive methods correct the phase errors after the fringe images are captured [17-20]. However, these techniques complicate the development of 3-D shape measurement system. Moreover, our experiments found that the projector nonlinearity changes overtime. On the contrary, if a technique can generate ideal sinusoidal fringe images without worrying about nonlinear gamma, it would significantly simply the development of the 3-D shape measurement system.

In this research, we will present the DBP approach to generate high-quality sinusoidal fringe patterns, which does not need projector nonlinear gamma calibration. This technique will be discussed next.

www.manaraa.com

2.5 Defocusing technique

Generally, the defocusing technique is to use a computer to generate binary structured images, and to defocus the projector to make them become sinusoidal structured ones. The defocusing is controlled by adjusting the focal length of the projector.

Figure 4 shows the binary structured pattern and its corresponding defocused one. A computer generates a binary structured pattern by setting pixels with two grayscale values 0 or 255. Figure 4(a) is the binary structured image which is projected onto a uniform white flat board and then captured by a camera when both the camera and projector are in focus. Figure 4(b) shows the 100^{th} row cross section of the binary structured image. It looks like a square wave. Figure 4(c) shows an example of the same pattern when the projector is defocused to a certain degree and the camera is focused. Figure 4(d) is its corresponding 100^{th} row cross section. The cross section shows that the square wave becomes a seemingly sinusoidal one. Thus, it seems to be feasible to generate ideal sinusoidal patterns by properly defocusing binary patterns.

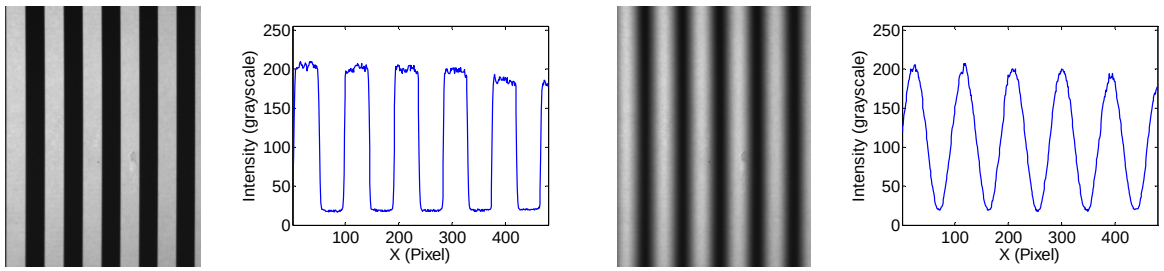

(a) (b) (c) (d)

Figure 4. (a) Example of a binary structured pattern when both the projector and camera are in focus; (b) 100^{th} row cross section of the pattern in (a); (c) Example of a defocusing binary structured pattern when the projector is defocused to a certain degree; (d) 100^{th} row cross section of the pattern in (c).

www.manaraa.com

(a) (b) (c) (d) (e)

(f) (g)

Figure 5. 3-D shape measurement of the sinusoidal fringe generation by defocusing binary structured patterns. (a) I_1 ; (b) I_2 ; (c) I_3 ; (d) Wrapped phase map; (e) Unwrapped phase map; (f)-(g) 3-D shapes viewed from different angles.

The DBP technique has been verified by measuring a complex sculpture, as shown in Figure 5. Figures 5(a)-(c) show three phase shifted fringe images with a phase shift of 2π/3. The 2π/3 phase shifting is realized by spatially moving 1/3 period of the binary structured patterns. Figure 5(d) is the wrapped phase map obtained from Equation (9). A phase unwrapping algorithm is applied to detect the 2π discontinuities and remove them by adding

www.manaraa.com

or subtracting multiples of 2π [33], Figure 5(e) shows the continuous unwrapped phase. In this research, the unwrapped phase is converted to coordinates by applying a phase-to-height conversation algorithm, which will be explained in the following Section 2.6. The results show that the proposed DBP approach can be used for measuring 3-D objects with complicated features.

2.6 Phase-to-height conversion algorithm

The obtained unwrapped phase contains the depth (*z*) information of the measured object, 3-D shape can be extracted from the unwrapped phase if the system is calibrated. In this research, we use a simple phase to height conversion algorithm.

To convert the phase to depth, the relationship between the depth and the phase must be established. Figure 6 shows the schematic diagram of the system. A reference plane with height 0 in the depth (*z* direction) is used as the reference for subsequent measurement. The arbitrary point *M* in the captured image corresponds to point *N* in the projected image, and point *D* on the object surface. From the projector's point of view, phase ϕ_D on the object surface has the same phase value as ϕ_A on the reference plane, that is, $\phi_D = \phi_A$. While from the point of view of the CCD camera, point *D* on the object surface images is at the same pixel as point *C* on the reference plane. The phase difference between point *C* on the reference plane and point *D* on the object can be expressed as:

$$\phi_{CD} = \phi_{CA} = \phi_C - \phi_A . \tag{11}$$

Assume the distance between point *M* and point *N* is *d* and the reference plane is parallel to the device with a distance *s* between them. By analyzing the similar relationship between $\triangle MND$ and $\triangle CAD$, we can get:

www.manaraa.com

$$\frac{d}{\overline{CA}} = \frac{s - \overline{BD}}{\overline{BD}} = \frac{s}{\overline{BD}} - 1. \tag{12}$$

Because for the real measurement, the distance s is much larger than $\overline{BD}$, the equation can be simplified as:

$$z(x, y) = \overline{BD} \approx \frac{s}{d}\overline{CA} = \frac{ps}{2\pi d}\phi_{CA} = K\phi_{CA}. \tag{13}$$

Here p is the distance per fringe on the reference plane. From Equation (13), the proportional relationship between the phase differences to height information (z coordinate) can be obtained.

We use a step to calculate the phase-height conversion constant K. The height of the step from the reference plane is approximately 53 mm. Figure 7(a) shows the 409th row cross section of the step height. The phase difference between the top and the bottom surface of the step is $\phi_{CA} = \phi_C - \phi_A$ = 6.4756 - 0.0838 = 6.3918 rad. The constant K is:

$$K = \frac{53}{6.3918} = 8.2919(mm/rad). \tag{14}$$

Assuming the x and y coordinate is proportional to the real coordinates of the object. The measured area on the reference plane is 144 × 187 mm^2, the conversion constant in x and y coordinates are:

$$k_x = k_y = \frac{187}{640} = 0.2922(mm/pixel). \tag{15}$$

Therefore, the 3-D coordinates of the object can be obtained by applying the conversion constant K, k_x, k_y onto the unwrapped phase of the object.

It should be noticed that this conventional reference-phase-based method still has some drawbacks, such as approximation errors, small range measurement, and inaccurate x

www.manaraa.com

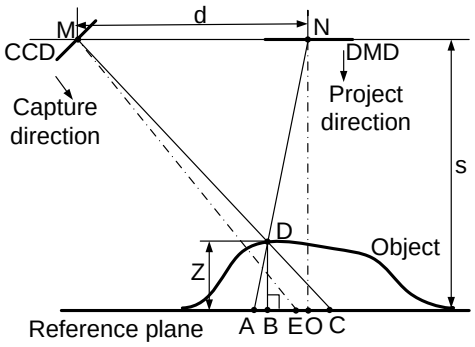

Figure 6. Schematic diagram of the phase-to-height conversion.

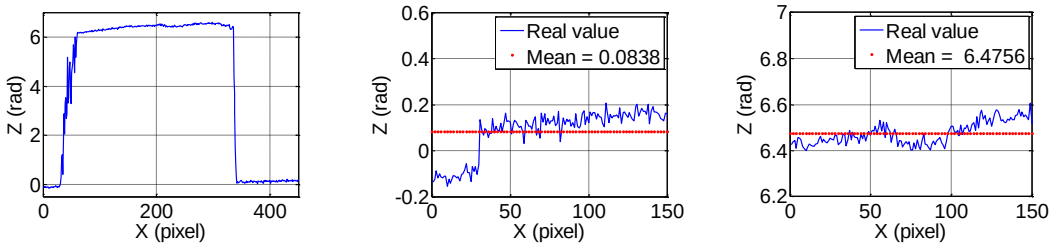

(a) (b) (c)

Figure 7. Measurement results of a flat board with a step. (a) 409th row cross section ofthe step; (b) Cross section of the bottom surface; (d) Cross section of the top surface.

and y coordinates [3]. At the current stage, all the existing techniques require the projector to be in focus, which is not the case for our system. We have not found a way to calibrate a defocused projector yet and we still use the standard simple calibration approach in our research. Currently, we are seeking a new method to accurately calibrate a defocused projector.

2.7 Summary

This chapter introduced the digital fringe projection technique, reviewed the three-step phase-shifting algorithm and phase-to-height conversion algorithm, and described the defocusing technique.

www.manaraa.com

CHAPTER 3. THEORETICAL BACKGROUND

In this chapter, we will introduce some optics background of the method used in this dissertation, including imaging system, Fourier optics, and Fraunhofer diffraction to better understand how defocusing works from the point of view of optics.

3.1 Imaging system

The lens system of a DLP projector can be modeled as a simple lens imaging system, as shown in Figure 8. All the rays, that are radiated by an object point are refracted by the convex lens, are converged to the corresponding points on the imaging plane. The irradiance and the position of the focused image of a point are uniquely determined, and the position of a point and its image are interchangeable. This means that the image of the image is the object itself.

For the lens of negligible thickness, in air, the relationship between the position of the point in the scene and the position of its corresponding focused image point can be explained as [35]:

$$\frac{1}{f}=\frac{1}{u}+\frac{1}{v}\ . \tag{16}$$

Where f is the focal length, u is the distance between the object and the lens, and v is the distance between the focused image and the lens plane. This formula indicates that as long as an object is placed at distance u ($u > f$) along the axis in front of a positive lens with focal length of f, a screen placed at a distance v behind the lens will have its corresponding image.

www.manaraa.com

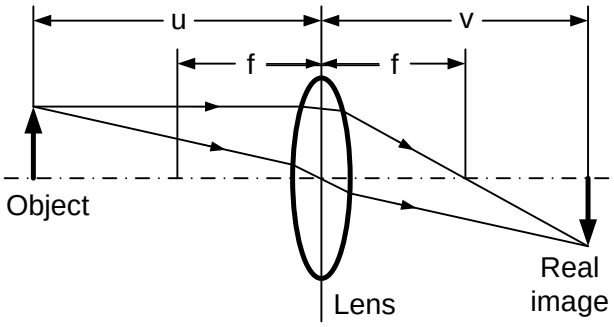

Figure 8. Imaging system in focus.

3.2 Fourier optics

The light source is composed of infinite point sources, and Fourier optics describes light propagation in terms of rays. In this section, we will firstly introduce some mathematical equations of light propagation, and then focus on the spherical wave, which will be used for the analysis of the Airy disk in Section 3.5.

Fourier optics is a branch of modern optics, which studies the classical optics using the Fourier analysis method in telecommunication theory. Telecommunication theory analyzes telecommunication signals, and only involves the Fourier transform of one-dimensional (1-D) time function. In optics, optical signal is a 3-D space function, the propagation of light in different directions with a spatial frequency needs Fourier transform of 3-D space function. Fourier optics spectrum analysis gives a new interpretation about a wide range of optical phenomena, which mainly includes scalar diffraction theory, imaging lens law, using spectral analysis to analyze the nature of the optical system, etc [36].

The propagation of light can be described as a waveform propagating through a vacuum or a material medium such as air or glass. Mathematically, the amplitude of the wave is expressed by a scalar wave function *u* which only depends on both space and time:

www.manaraa.com

$$u = u(\vec{r}, t)\,. \tag{17}$$

Where $\vec{r} = (x, y, z)$ is the position in 3-D space, and t represents time. The wave equation in the time domain can be represented as follows [37]:

$$(\nabla^2 - \frac{1}{c^2}\frac{\partial^2}{\partial t^2})u(\vec{r}, t) = 0 \tag{18}$$

.

Where $u(\vec{r}, t)$ is a real value Cartesian component of electromagnetic wave propagation through a vacuum, c is a fixed constant equal to the propagation speed of the wave, and ∇ is the Laplacian operation.

In Fourier optics, light is assumed as a fixed frequency, and the optical field is given as:

$$\psi(\vec{r}) = a(\vec{r})e^{j\phi(\vec{r})}\ . \tag{19}$$

Where ψ is in general a complex quality with separate amplitude and phase.

For the light emitted from a point source, if the wave surface is spherical wavefront, it is called spherical waves. Figure 9 shows a divergent spherical wave. Spherical wave of the same phase is a set of concentric spherical surfaces, and the amplitude of each point is inversely proportional to the distance from the point to the center of sphere. The amplitude of any monochromatic spherical wave generated by source point P is given in this form:

$$U(P) = \frac{a_0}{r}e^{j\vec{k}\bullet\vec{r}}\ . \tag{20}$$

Where $\vec{r}$ is the radius vector of point P, and $r = |\vec{r}| = \sqrt{x^2 + y^2 + z^2}$, a_0 is the amplitude at $r = 1$, $\vec{k}$ is wave vector, and $k = |\vec{k}| = \frac{2\pi}{\lambda}$, the size of k is called as spatial angular frequency.

www.manaraa.com

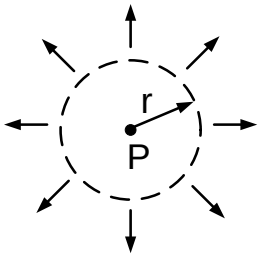

Figure 9. Divergent spherical wave.

3.3 Fraunhofer diffraction

Equation (16) is based on geometrical optics, which does not consider the light diffraction. Light diffraction occurs when the light passes through a small opening, comparable in size to the wavelength λ of the light, in an otherwise opaque obstacle, the wavefront on the other side of the opening resembles the wavefront shown in Figure 10.

Diffraction is a wave after the obstacle of the holes continues to spread through the phenomenon of scattering. Fraunhofer diffraction is a form of wave diffraction that occurs when field waves are passed through a slit causing only the size of an observed aperture image to change.

In scalar diffraction theory, the Fraunhofer approximation is a far field approximation, and the diffraction equation is [38]:

$$U(x,y)=\frac{\exp(jkz)}{j\lambda z}\exp\left[jk\left(\frac{x^2+y^2}{2z}\right)\right]\iint_{-\infty}^{\infty}U_0(x_{0,}y_0)\exp\left[-j\frac{2\pi}{\lambda z}\left(x_0x+y_0y\right)\right]dx_0dy_0 \qquad (21)$$

Where $U_0(x_{0,}y_0)$ is the optical field distribution of diffraction aperture plane, k is spatial angular frequency, (x,y,z) and (x_0,y_0,z_0) are the coordinates of a diffraction aperture plane and an observation plane, respectively.

www.manaraa.com

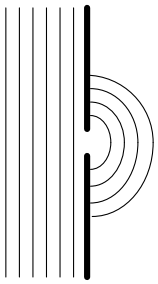

Figure 10. Optics wave diffraction.

3.4 Point spread function

In imaging system, point spread function (PSF) is defined as the radiation intensity distribution in the image to an infinitely small point source [39]. A more general term for the PSF is a system's impulse response, the PSF being the impulse response of a focused optical system. In a perfect imaging system, the radiant energy generating from an infinitely small point source in the object plane would be concentrated at an ideal point in the image plane, which is called the ideal image point. However, in practical systems, there is a "smearing-out" of the energy around the ideal point image, which results in unsharp imaging of the point source. The PSF is a way of measuring such unsharpness [40].

Mathematically, if there is no distortion in the imaging system, the image plane coordinates are linearly related to the object plane coordinates via the magnification *M* as:

$$(x_i, y_i) = (Mx_0, My_0). \tag{22}$$

The object is divided into discrete point objects of different intensity, and the ideal point can be assumed as a 2-D impulse function, then the object plane field can be represented as:

$$O(x_0, y_0) = \iint O(u,v)\delta(x_0 - u, y_0 - v)dudv. \tag{23}$$

www.manaraa.com

This means that the object is a weighted sum over impulse functions. According to the superposition principle, the image plane field is the superposition of the image of each of the individual impulse functions. Then the image is expressed as:

$$I(x_i, y_i) = \iint O(u,v)PSF(x_i - Mu, y_i - Mv)dudv \ . \tag{24}$$

In which, $PSF(x_i - Mu, y_i - Mv)$ is the imaging of the impulse function $\delta(x_0 - u, y_0 - v)$. Equation (24) indicates the image of an object can then be seen as a convolution of the true object and the PSF.

3.5 Airy disk

In focusing imaging system, Airy disk and Airy pattern are descriptions of the best focused spot of light that a perfect lens with a circular aperture can make. Therefore, the real image we can get is a convolution of the ideal image with the Airy disk pattern [41]. Mathematically, the Airy disk is given by the Fourier transform of the circle aperture:

$$I(\theta) = I_0 \left\{ \frac{2J_1(ka\sin(\theta))}{ka\sin\theta} \right\}^2 = I_0 \left[\frac{2J_1(x)}{x} \right]^2, \tag{25}$$

$$J_1(x) = \sum_{m=0}^{\infty} \frac{(-1)^m}{m!\Gamma(m+2)} \left(\frac{x}{2} \right)^{2m+1}, \tag{26}$$

$$\Gamma(x) = \int_0^{\infty} t^{x-1} e^{-t} dt \ . \tag{27}$$

Where, I_0 is the maximum intensity of the pattern at the Airy disk center, J_1 is the Bessel function of the first kind of order 1, Γ is the gamma function, $a = d/2$ is the radius of the aperture, $k = 2\pi/\lambda$ is the wave number, and θ is the angle between the axis of the circle

www.manaraa.com

aperture and the line between the aperture center and the observation point, as shown in Figure 11.

Limited by diffraction theory, the angle of the Airy disk is given by:

$$\sin(\theta) = 1.22\frac{\lambda}{d}. \tag{28}$$

Here, λ is the wavelength of the light, and d is the diameter of the aperture.

Figure 11 shows the schematic diagram of the imaging system with a finite size lens. The point light source emits an ideal spherical waves, and is imaged by the lens onto its imaging plane. In practice, due to the finite size of the lens and light diffraction, the image of a point object is not a crisp circular patch of constant brightness, as suggested by geometrical optics. Instead, it will be roughly a circular blob with the brightness falling off gradually with increasing distance from the center, as shown in Figure 12 and Figure 13. The image point appears to be an Airy disk as shown in Figure 11, and the fractions of the total power contained with the first dark ring is 83.8%.

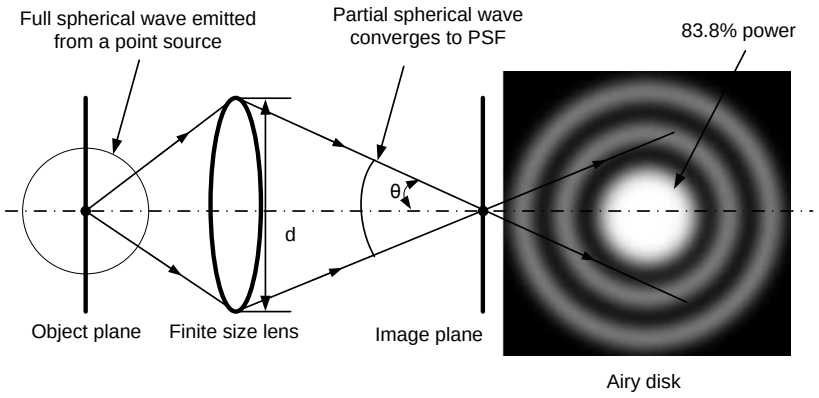

Figure 11. Finite size lens imaging system generates an Airy disk from point light source with spherical waves.

www.manaraa.com

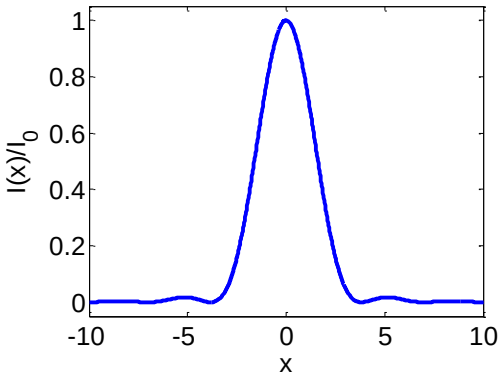

Figure 12. The Airy pattern with the interval x = kasin(θ) ∈ [-10,10].

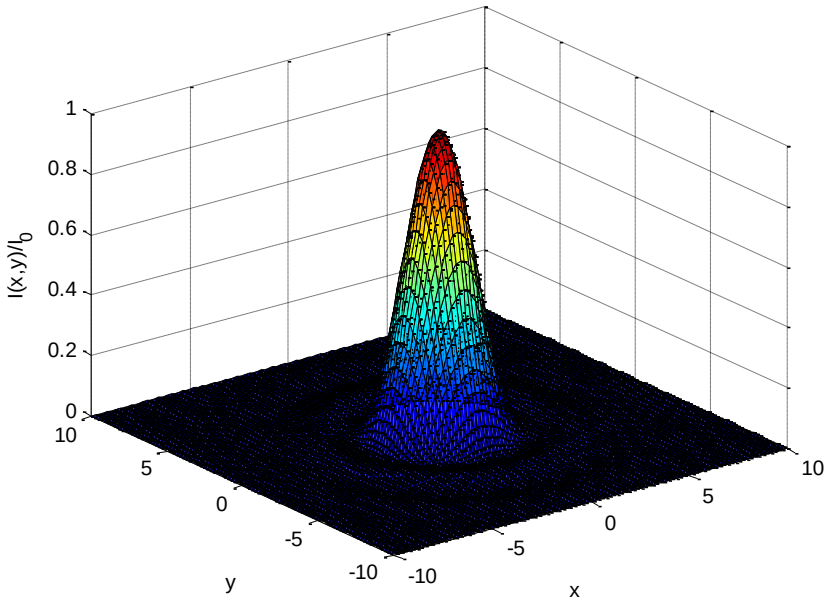

Figure 13. Surface plot of the intensity of an Airy disk.

3.6 Model of defocus

The image information introduced previously tells how an image is generated when the imaging system is in focus. That is, when a point light source is in focus, all rays that are radiated from the object point and intercepted by the lens converge at a point on the image

www.manaraa.com

plane. However, when the system is out of focus, the image on the image plane is no longer a focused point but a blurred circular whose radius σ' describes the amount of defocus associated with the depth of the point in the scene [42].

$$\sigma' = \rho r v' \left| \frac{1}{f} - \frac{1}{v'} - \frac{1}{u} \right| . \tag{29}$$

Where ρ is a constant related with the imaging system, r is the radius of the lens aperture, v' is the lens-to-image distance, f is the focal length of the lens, and u is the distance of the object point from the lens. Figure 14 shows the imaging system in defocus.

Mathematically, the Airy disk can be expressed in Equation (25). From Figure 12, we can see the Airy pattern falls rather slowly to zero with increasing distance from the center, with the outer rings containing a significant portion of the integrated intensity of the patterns. An alternative way to approximate the Airy disk pattern is to ignore the relatively small outer rings of the Airy pattern, and to use a Gaussian profile to approximate the central lobe. 1-D Gaussian function is expressed in the following form:

$$f(x) = \frac{1}{\sqrt{2\pi}\sigma} \exp\left[-\frac{(x-\mu)^2}{2\sigma^2} \right]. \tag{30}$$

Where, μ is the expected value and σ is the standard deviation.

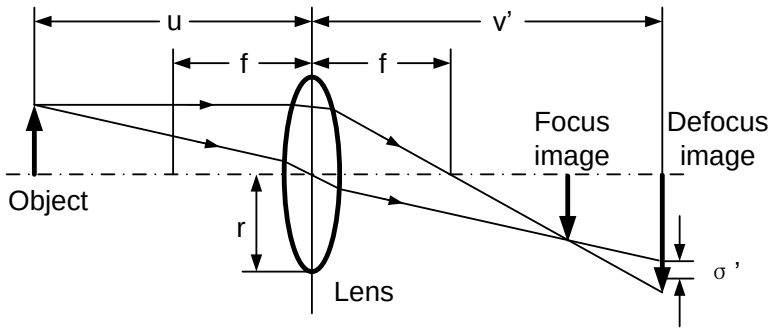

Figure 14. Imaging system in defocus.

www.manaraa.com

Figure 15 shows that the Gaussian has a characteristic symmetric "bell curve" shape that quickly falls off towards infinity. The parameter μ is the position of the center of the peak, and σ controls the width of the "bell".

If we equate the peak amplitude of the Airy pattern and Gaussian profile to be equal, and find the value of σ giving the optimal approximation to the pattern [41], we obtain:

$$\sigma \approx 0.42 \frac{\lambda f}{D}. \tag{31}$$

Where f is the focal length of the imaging system, λ is the wavelength, and D is the diameter of the entrance pupil.

Figure 16 shows the radial cross-section through the Airy pattern and its Gaussian profile approximation. From this figure, we can see the Gaussian profile is a good approximation to the Airy disk pattern.

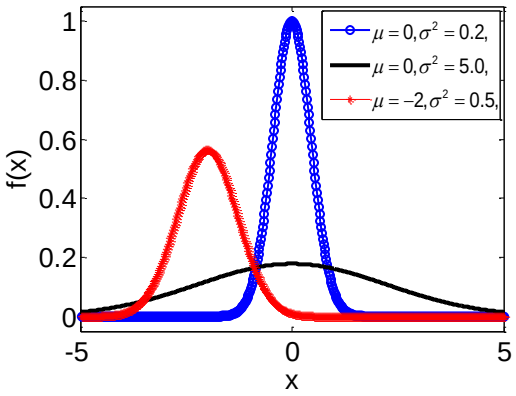

Figure 15. Gaussian curve with expected value μ and variance σ^2.

www.manaraa.com

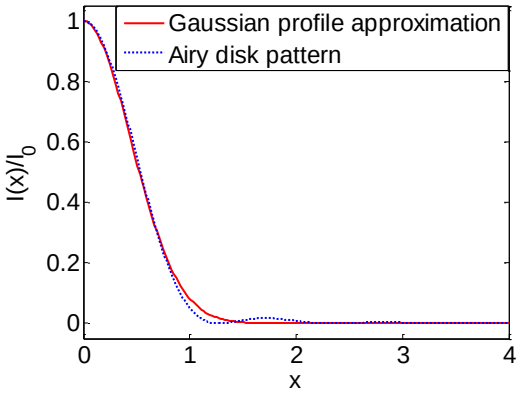

Figure 16. A radial cross-section through the Airy pattern and its Gaussian profile approximation. The Gaussian curve with expected value μ =0 and variance σ^2 = 0.2, and the Airy pattern with the interval x = kasin(θ) ∈ [0, 4].

An analysis shows that the sum of the various functions obtained at different wavelengths has the general shape of a 2-D Gaussian function [43]. Thus, for a diffraction-limited lens system, the PSF of the imaging system can be approximated as a circularly symmetric 2-D Gaussian function [42].

$$h(x,y) = \frac{1}{2\pi\sigma'^2}\exp\left(-\frac{x^2+y^2}{2\sigma'^2}\right). \tag{32}$$

Here the blur parameter σ' is defined from Equation (29). Therefore, the image $I(x,y)$ becomes the convolution of the focused image $F(x,y)$ with the corresponding PSF $h(x,y)$.

$$I(x,y) = F(x,y) \otimes h(x,y). \tag{33}$$

www.manaraa.com

3.7 Summary

This chapter introduced some optical theory used in this dissertation: image system, Fourier optics, Fraunhofer diffraction, point spread function, Airy disk, and model of defocus. The goal is to give some optics background on how an image is generated when the image system is in focus or defocus. Next, we will introduce how to use a Gaussian filter to simulate the defocusing effect and show some simulation results.

www.manaraa.com

CHAPTER 4. SIMULATION

In this chapter, we will introduce the mathematical representation of the binary patterns, and then simulate the defocusing effect by applying a Gaussian filter. Finally, we will show some simulation results.

4.1 Theoretical analysis

Mathematically, a binary pattern generated by a computer can be regarded as a square wave horizontally, and the imaging system can be regarded as a PSF [40]. The defocusing of the projector will generate blurred images. The degree of defocusing can be modeled as a different breadth of PSF. The PSF can be approximated as a Gaussian smoothing filter [41]. If a filter is applied so that only the first harmonics is kept, an ideal sinusoidal waveform will be produced.

Because the structured patterns have vertical stripes with exactly the same structure, in order to understand how the binary pattern changes when the projector is defocused, we only need to understand how one horizontal cross section of the pattern alters. Mathematically, the cross section of the binary pattern can be considered as a square wave, which can be written in the following form:

$$y(t)=\begin{cases}0 & t\in[nT-T/2,nT]\\ 1 & t\in[nT,nT+T/2]\end{cases}. \tag{34}$$

Where, T is the period, n is an integer. In the Fourier domain, the square wave can be represented as:

www.manaraa.com

$$y(t) = 0.5 + \sum_{n=0}^{\infty} \frac{2}{(2n+1)\pi} \sin\left[\frac{2\pi(2n+1)}{T} t\right] \quad (35)$$

.

From Equation (35), we can see that the square wave only has odd harmonics without even ones, thus, it is easier to design a filter to suppress the higher-frequency components. This explains the feasibility of generating sinusoidal structured patterns by properly defocusing binary ones. If the binary structured patterns are moved horizontally, phase-shifted fringe patterns with sinusoidal fringe patterns will be generated after defocusing. Thus, this approach can be used for 3-D shape measurement by using a digital fringe projection and phase-shifting method.

4.2 Simulation results

To understand how the degree of defocusing affects the measurement error, we simulate the defocusing effect by applying a Gaussian smoothing filter. The degree of blur can be modeled as applying different widths of the Gaussian smoothing filter, and different degrees of defocusing can be realized by applying different sizes of filters or the same size of filters at different number of times. The latter approach is adopted in this research. This is because the convolution of two Gaussian functions is another Gaussian function [44], which can be expressed in the following form:

$$\frac{1}{\sqrt{2\pi}\sigma_1} \exp\left[-\frac{(x-\mu_1)^2}{2\sigma_1^2}\right] \otimes \frac{1}{\sqrt{2\pi}\sigma_2} \exp\left[-\frac{(x-\mu_2)^2}{2\sigma_2^2}\right] = \frac{1}{\sqrt{2\pi(\sigma_1^2+\sigma_2^2)}} \exp\left[-\frac{[x-(\mu_1+\mu_2)]^2}{2(\sigma_1^2+\sigma_2^2)}\right]. \quad (36)$$

Here, μ_1 and μ_2 are expected values, σ_1 and σ_2 are standard deviations.

www.manaraa.com

In this simulation, because the structured stripes are either vertical or horizontal, only one cross section perpendicular to the fringe stripes needs to be considered. Thus, the problem is reduced to 1-D filter expressed as Equation (30).

Figure 17(a) shows the cross section of a binary structured pattern (square wave) with the period of 48 pixels, and then after applying a Gaussian filter with 7 pixels and a standard derivation of 3.5 pixels. The sharp edges of the binary patterns start softening and the square wave becomes trapezoidal in shape, as shown in Figure 17(b). If the same filter is applied again, the waveform is close to sinusoidal, but the top and the bottom remain flat, as shown in Figure 17(c). Figure 17(d)-(f) show the results when the filter is applied the third, fourth, and fifth times. It clearly shows that the wave becomes more and more sinusoidal when the defocusing degree increases. One should notice that the amplitude of the sinusoidal wave decreases as the degree of defocusing increases. This indicates that the fringe contrast drops accordingly. For a real measurement system, this may result in larger error because the quantization error of a digital camera is larger. For this simulation, a floating point is used to reduce the error caused by quantization.

The phase shifting is simulated by spatially moving the binary patterns. For example, a $2\pi/3$ phase shifting can be realized by moving 1/3 period of the binary patterns. With generating three phase-shifted fringe patterns, the phase value can be computed by applying Equation (9). A phase unwrapping algorithm is used to remove 2π discontinuities and obtain a continuous phase map. In this simulation, we use a Matlab function to unwrap the phase:

$$\Phi(x,y) = \phi(x,y) + 2\pi \times m(x,y) \quad . \tag{37}$$

Here, ϕ is the phase obtained from Equation (9), and Φ is the continuous unwrapped phase.

www.manaraa.com

And then, the first polynomial is used to obtain the general profile (slope) of the unwrapped phase. The phase error is computed by subtracting the unwrapped phase by the slope.

Figure 18 shows the corresponding phase error for the smoothed fringe images shown in Figure 17. The phase error for a square wave is very large, and root mean square (RMS) is 0.3307 or 0.3007/ $(2\pi) \times 100\% \approx 4.8\%$, as shown in Figure 18(a). On the contrast, when the filter is applied the second, third, fourth, and fifth times, seen in Figures 17(c)-(f), the profile of the fringe becomes more sinusoidal, and the phase error reduces to less than 0.06%, which can be negligible. Therefore, once the binary structured patterns are defocused to be

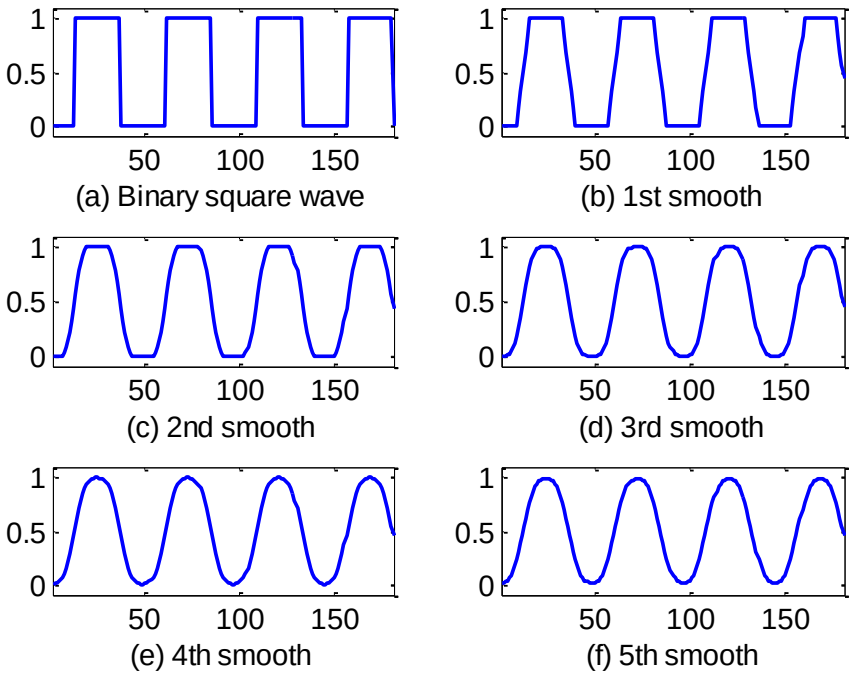

Figure 17. Schematic diagram of the cross section of a binary structured pattern when applying a Gaussian smoothing filter at different times. The period of binary square wave is 48 pixels, and the standard derivation of the Gaussian filter is 3.5.

www.manaraa.com

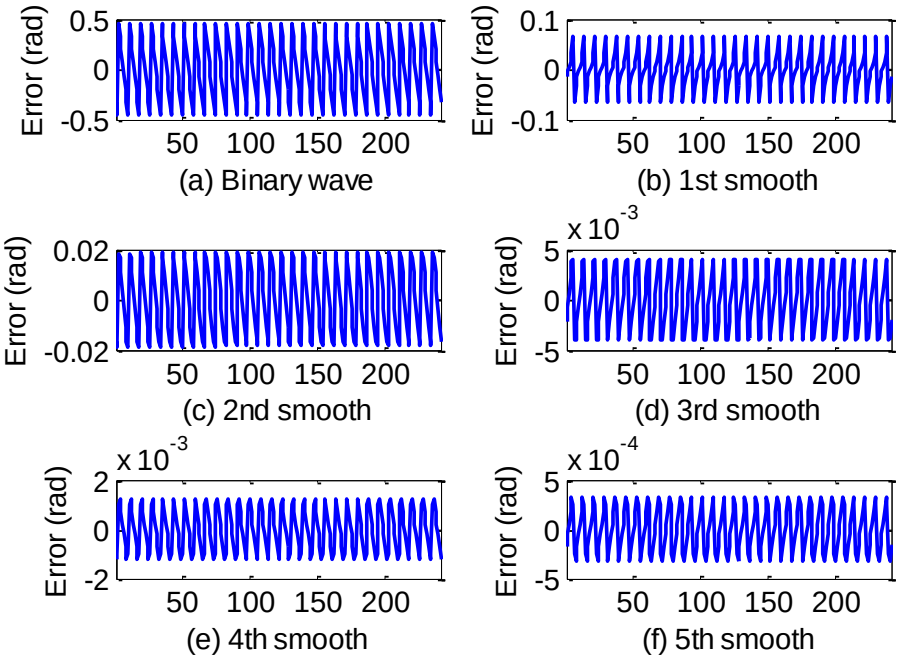

Figure 18. RMS phase error for different smoothing levels from (a)-(f) are 0.3007, 0.0375, 0.0138, 0.0030, 0.0009, 0.0002 rad, respectively.

sinusoidal ones, further defocusing will not significantly increase the phase error. From Figures 17(a)-(f), we can find the amplitude of the wave gradually becomes smaller as the defocusing degree increases. That means the fringe contrast will reduce gradually. Actually, in a real 3-D shape measurement system, if the degree of defocusing is too low, fringe contrast will be very low. Even though some fringe enhancement techniques can be used [45], the random noise will bring significant error into the phase.

Since nonsinusoidal waveforms usually result in periodical phase error. It should be noted that the phase error shown in Figure 18 appears to be periodical. There may be two reasons to explain the periodical phase error. One is the finite filter size of the Gaussian filter. However, in the real measurement system, the lens defocusing acts as an analog device,

www.manaraa.com

which will not involve the problems caused by discrete filtering. Another reason may be the high order harmonics components.

4.3 Summary

This chapter first introduced the mathematical equations of the binary patterns, and then, to better understand how the defocusing degree affects the measurement error, we simulated the defocusing effect by applying a Gaussian filter. Finally, some simulation results and analysis were shown.

www.manaraa.com

CHAPTER 5. EXPERIMENTAL RESULTS AND DISCUSSIONS

In this chapter, we will compare the performance of the new DBP approach against the traditional FSP method by analyzing the phase errors introduced by the following factors: (1) degree of defocusing, (2) exposure time, (3) synchronization, and (4) projector nonlinear gamma. Experimental results show that in most scenarios, the error for the DBP method is smaller than that of the FSP method. Next, we will show some 3-D reconstruction results of complex objects by using the DBP and the FSP methods respectively. Finally, we will summarize the work and discuss the results.

5.1 Test system

The performance of the proposed approach was verified with a structured light system, as shown in Figure 19. The system includes The Imaging Source Digital USB CCD camera (DMK 21BU04) with Computar M0814-MP lens F/1.4 with f = 12 mm, and the Dell projector (M109S). The camera resolution is 640 × 480, with a maximum frame rate of 60frames/sec. The minimum and maximum exposure times of the camera are 0.1 ms and 30 sec, respectively. The pixel size of the camera sensor is 5.6 × 5.6 μm^2. The projector has a resolution of 858 × 600 with a lens of F/2.0, f = 16.67 mm. The projection distance is 599.4-2400.3 mm. The DMD used in this projector is 11.43-mm Type Y chip.

This projector uses Texas Instrument BrilliantColor^{TM} technology to enhance the brightness and color gamut [46]. In this technology, instead of using red, green, blue (RGB) three colors, it uses five colors including yellow and cyan to use coupling spectra between RG and GB. To simplify the test, only the green channel is used for tests.

www.manaraa.com

Figure 19. Photograph of the test system.

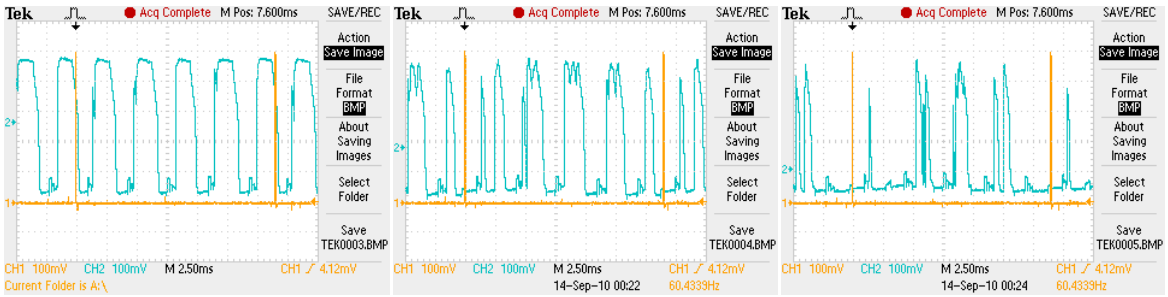

(a) (b) (c)

Figure 20. Projector timing signal if the projector is fed with different grayscale values of the green image. (a) 255; (b) 128; (c) 64.

To understand how the projector projects images, we send different grayscale values of the green images to the projector and use a photodiode to sense the output light, and then the photocurrent is converted to a voltage signal and monitored by an oscilloscope. Figure 20 shows the results displayed on the oscilloscope. Channel 1 shows VSync of the video graphics array (VGA) signal connected with the projector and channel 2 of the oscilloscope shows the detected signal. Because the projector is synchronized with the computer's video signal through VSync, its projection cycle is 1/60 s. If the pure green RGB = (0, 255, 0) image is supplied to the projector, there are five periods of signal output for each VSync period (1/60 s) and the signal is almost filled in during each channel duration (approximate

www.manaraa.com

16.67 ms), as shown in Figure 20(a). When the grayscale value is reduced to 128, approximately half of the channel is filled, as shown in Figure 20(b). If the input grayscale is reduced to 64, only a smaller portion of the channel is filled, as shown in Figure 20(c).

Comparing the results from Figure 20, it seems that if the grayscale value is somewhere between 0 and 255, the output signal becomes irregularly, and we cannot use any portion signal to represent the whole signal. Therefore, for the FSP method, when the projector is supplied with sinusoidal fringe patterns with the intensity varying from 0 to 255, the camera must capture the whole projection period to obtain the correct image projected from the projector. This would bring two problems in the 3D shape measurement by using the FSP method. One is the exposure time limitation problem; another is the synchronization problem between the projector and the camera. These two problems will be discussed in Section 5.3 and Section 5.4, respectively.

5.2 Defocusing degree

The simulation results introduced in Section 4.2 show that it is feasible to generate sinusoidal fringe patterns by defocusing binary patterns. Theoretically, we can find a proper defocusing degree to generate high-quality sinusoidal structured patterns. Therefore, to compare the phase error at various defocusing degrees, 5 levels of defocusing are tested. During the experiments, a uniform flat surface is imaged, and the camera is synchronized with the projector through VSync signal of computer video. The exposure time is set to be one projection cycle (i.e., 16.67ms). The camera is always in focus during the test. The projector starts in focus and then increases its defocusing degree by adjusting the focal length of the projector. For the traditional method, the gamma of the projector is calibrated and the

www.manaraa.com

associated phase error is compensated.

Figures 21(a)-(e) show examples of the fringe images captured when a binary structured pattern is sent to the projector and the projector is defocused at different levels. Figures 21(f)-(j) show the corresponding 100^{th} row cross sections in above corresponding images. At level 1, both the projector and the camera are in focus, therefore for the DBP method the fringe patterns have very obvious binary structures, as shown in Figure 21(a). With the increase of the defocusing degree, the binary structures are less and less clear, and they become more and more sinusoidal. Figure 21(c) shows sinusoidal fringe stripes, thus, it seems to be feasible to generate ideal sinusoidal patterns by properly defocusing binary patterns. However, if the defocusing degree is too much, sinusoidal structure becomes obscure and the contrast of the fringe image is low, as shown in Figure 21(e). From Figures 20(a)-(e), we can see the binary structured patterns become sinusoidal ones when the defocusing degree increases and contrast of the fringe images gradually becomes low.

Figures 21(k)-(o) show the sinusoidal fringe images generated by the FSP method and the corresponding cross sections. Figure 21(k) shows the result when the projector is in focus, and Figures 21(l)-(o) show the results when the projector is increasingly defocused. Compared with the results in Figures 21(a)-(e), when the projector is supplied with a sinusoidal pattern, the fringe image has very high contrast when the projector is in focus, as shown in Figure 21(k). However, when the projector is defocused, the fringe contrast is lower than its DBP counterpart. When the projector is defocused to a degree, the fringe quality for the DBP method is better than that for the FSP method.

Once three phase-shifted images are captured, the phase value can be obtained by using Equation (9). A phase unwrapping algorithm is used to remove the 2π discontinuities

www.manaraa.com

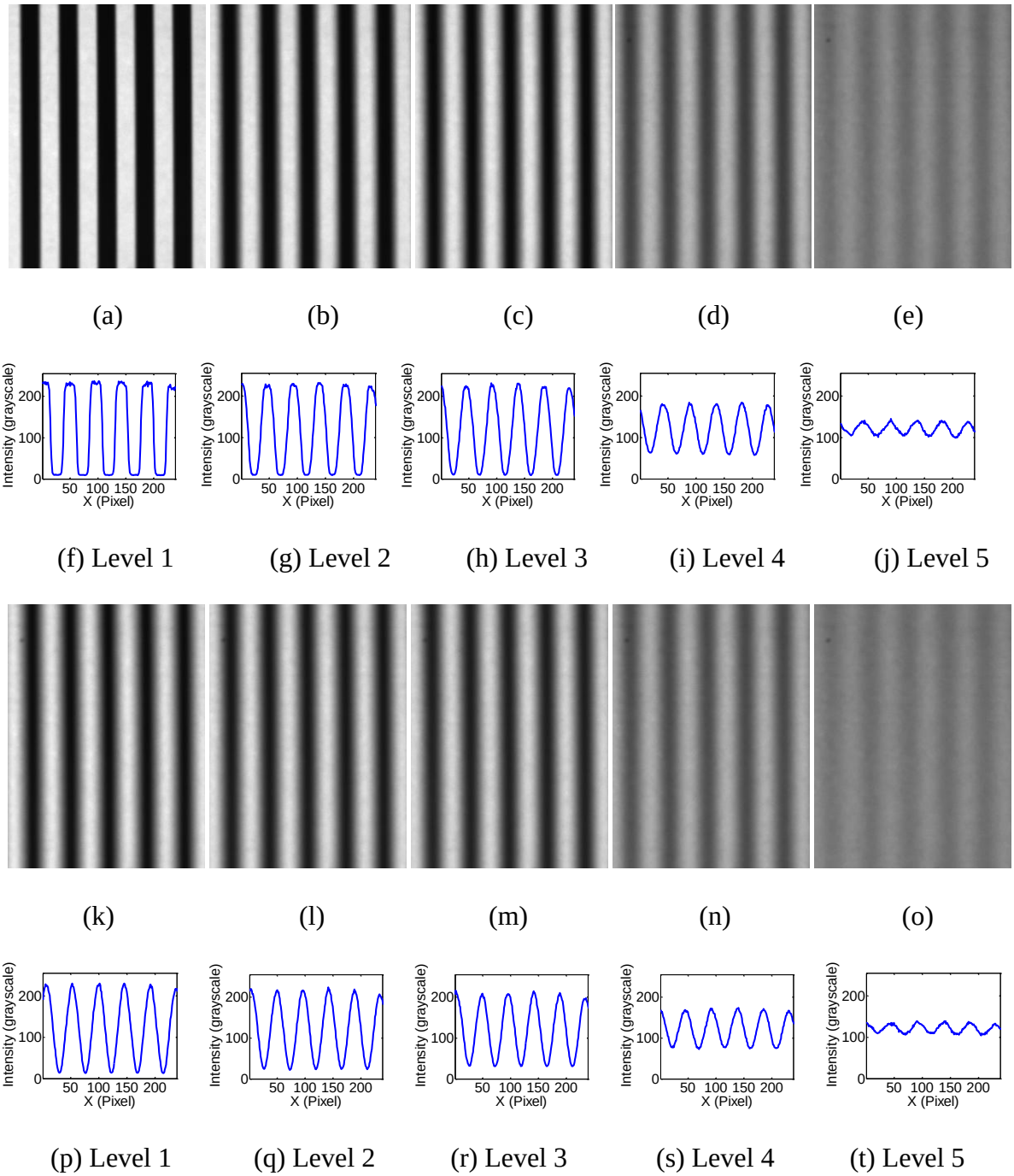

Figure 21. Example of fringe images (a)-(e) and the 100th cross section (f)-(j) of the fringe images for the DBP method at different defocusing levels. Example of fringe images (k)-(o) and the 100th cross section (p)-(t) of the fringe images for the FSP method at different defocusing levels. Level 1 is focus and level 5 is severely defocused.

www.manaraa.com

to obtain a continuous phase map, and its slope is removed to better show the phase error. For the FSP method, a nonlinear gamma calibration method [16] is adopted to ensure the projector project ideal sinusoidal fringe images.

The associate phase errors are plotted in Figure 22. Figures 22(a)-(e) show the phase error when the DBP is used. We can see if both the projector and the camera are in focus, the phase error is very large (RMS 0.106 rad). When the defocusing degree increases gradually, fringe patterns will become much more sinusoidal and the phase error becomes much smaller (RMS in Figure 22(c) is 0.020 rad). However, if the defocusing degree is too large, the sinusoidal structure becomes obscure, and the phase error increases again. This experiment shows that there is a large range of defocusing when the phase error is relatively small. Therefore, the DBP method can be used for generating sinusoidal fringe pattern with a large depth range.

Figures 22(f)-(j) show the phase error when the FSP method is used. When the projector is in focus, no obvious periodical error appears, and the phase error is very small (RMS 0.019 rad). This is because the gamma of the projector is calibrated and the associated phase error is compensated well. However, when the projector begins defocusing, periodical error appears. The error seems to be caused by a single-frequency component and the signal frequency component is usually the result of the imbalance of the three fringe images. There may be two reasons to explain the periodical error when the projector is defocused. (1) It is not easy to precisely represent the gamma of the projector using a mathematical equation by calibration, because it is a complicated curve; and (2) it could be the precision of the synchronization between the projector and the camera, which will be explained in Section 5.4.

www.manaraa.com

As a comparison, the phase error generated by the DBP method is smaller when the projector starts defocusing.

Figure 23 shows the phase error introduced by these two methods under different defocusing degrees. From this figure, we find that when the projector is in focus, the traditional method works better, and the phase error caused by the FSP method (RMS 0.019 rad) is much smaller than that in the DBP method (RMS 0.106 rad). However, when the projector is defocused to a degree, the phase error induced by the DBP method is actually smaller than that produced by the FSP method, which means the proposed method starts outperforming the traditional one. It is interesting to notice that both methods produce similar phase error under their own best conditions. This experiment clearly indicates that it is possible to generate ideal sinusoidal fringe patterns by defocusing binary patterns.

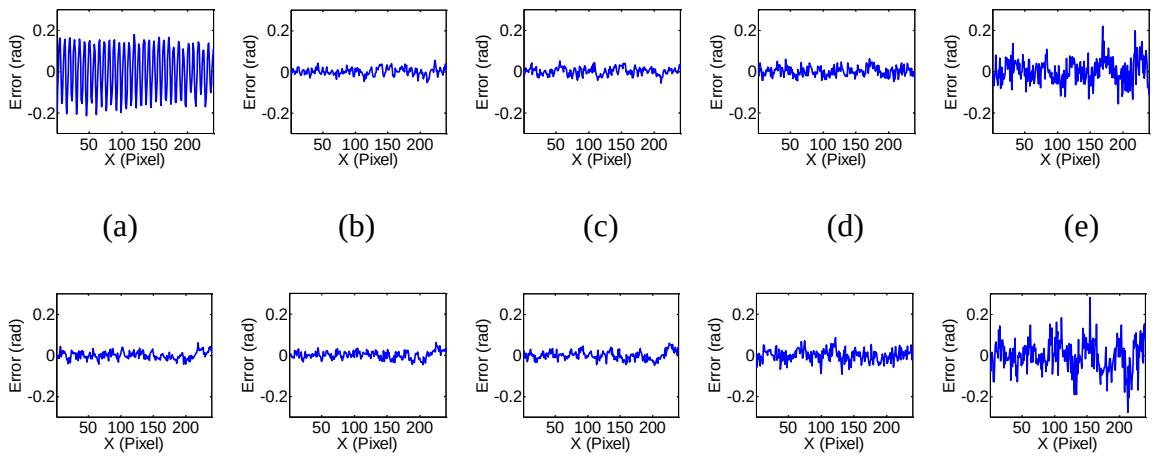

Figure 22. (a)-(e) Phase error for different defocusing levels of fringe images is shown in Figure 21(a)-(e). The RMS errors in (a)-(e) are 0.106, 0.022, 0.020, 0.024, 0.073 rad; (f)-(j) Phase error for different defocusing level of fringe images is shown in Figure 21(k)-(o). The RMS errors in (f)-(j) are 0.019, 0.019, 0.021, 0.033, 0.109 rad.

www.manaraa.com

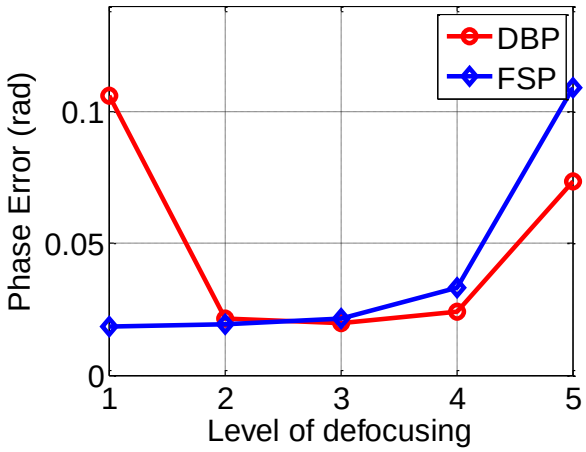

Figure 23. Phase errors for different defocusing levels of fringe images in Figure 21.

A complex object is measured with both the DBP method and the FSP method. In this research, the $2\pi/3$ phase shifting is realized by spatially moving 1/3 period the fringe patterns. The phase is converted to coordinates by applying a phase-to-height conversion algorithm introduced in Section 2.6, and the 3-D geometry is smoothed by a 5×5 Gaussian filter to reduce the most significant random noises.

To compare the 3-D measurement quality at various defocusing degrees, 4 levels of defocusing are tested. Figure 24 shows the measurement results of a complex sculpture for the DBP and the FSP methods at different defocusing levels. Figures 24(a)-(d) show the 3-D shape by the DBP method with defocusing levels from 1 to 4, and Figures 24(e)-(h) show the 3-D reconstruction results by the FSP method at the same levels as above. At level 1, both the projector and the camera are in focus. 3-D reconstruction by the DBP method has a very large error, as shown in Figure 24(a), while for the FSP method, it gets a high-quality 3-D shape, as shown in the Figure 24(e). With the defocusing degree increasing, the DBP method gradually gets better results, as shown in Figures 24(b)-(c). However, if the defocusing degree is too great, the measurement quality drops. On the contrast, for the FSP method,

www.manaraa.com

when the projector is focused, it gets a high-quality shape, as shown in Figure 24(e). With the increase of the defocusing degree, the measurement quality drops, as shown in Figures 24(f)-(h). These experimental results clearly indicate it is feasible to get high-quality 3-D reconstruction results by the DBP method as long as the projector is properly defocused.

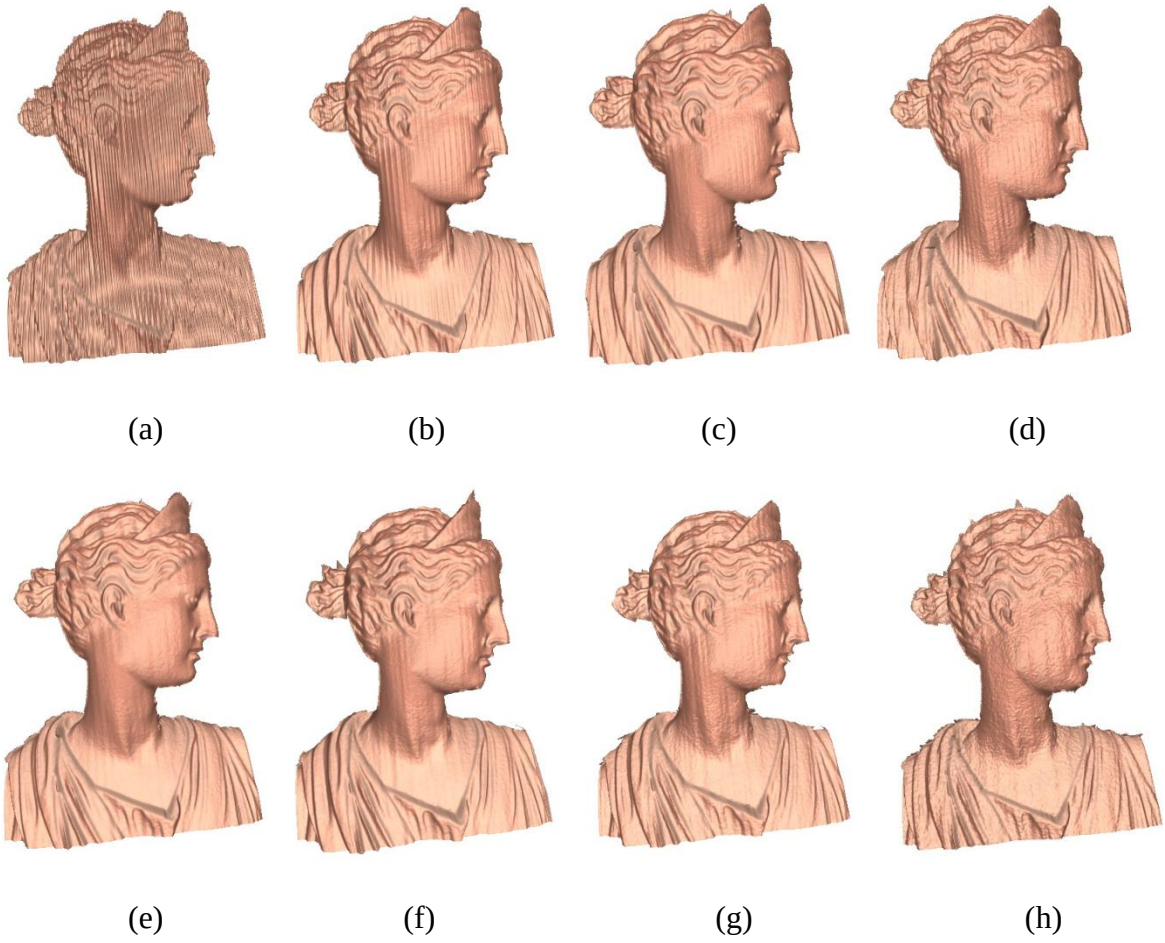

Figure 24. Measurement results of a complex sculpture for the DBP and the FSP methods at different defocusing levels. Level 1 is focused and level 4 is severely defocused. (a)-(d) show the results by the DBP method with defocusing levels from 1 to 4, and (e)-(h) show the results by the FSP method with different levels.

www.manaraa.com

5.3 Exposure time

Short exposure time is especially needed when measuring very fast motion. To evaluate how the camera's exposure time influences the measurement, 15 different exposure times are tested and the phase errors are calculated accordingly. During this experiment, a uniform flat surface is imaged. The camera is always in focus and synchronized with the VSync signal of the computer video. For the DBP method, the projector is properly defocused to a certain degree to generate high-quality sinusoidal fringe patterns. For the FSP method, the projector is in focused and gamma calibration is applied to ensure the projector to project ideal sinusoidal fringe patterns.

When the exposure time is less than one channel projection, 10 different exposure times (2.50, 4.17, 5.83, 7.50, 9.17, 10.83, 12.50, 14.17, 15.80, 16.67 ms) are used for data acquisition. The exposure time is selected so that either partial or the whole projection pulse can be captured by the camera. For simplicity, only the green channel is used, and the projector uses the BrilliantColor^{TM} technology, five pulses are generated within one projector cycle, as shown in Figure 20(a). The camera is synchronized with the computer's video signal through VSync, the camera always starts its exposure time when the VSync signal comes and stops at different timing, as shown in Figure 25. Because the camera's exposure time changes, aperture is adjusted accordingly to achieve high quality fringe images during the test.

For the FSP method, the projector is in focus, and the nonlinear gamma of the projector is calibrated to reduce the phase error. Figure 26(a) shows the fringe image when the exposure time is set to be 2.5 ms. From this figure, the nonsinusoidal patterns are clearly displayed, that is because compared with one projector cycle of 16.67 ms, the exposure time

www.manaraa.com

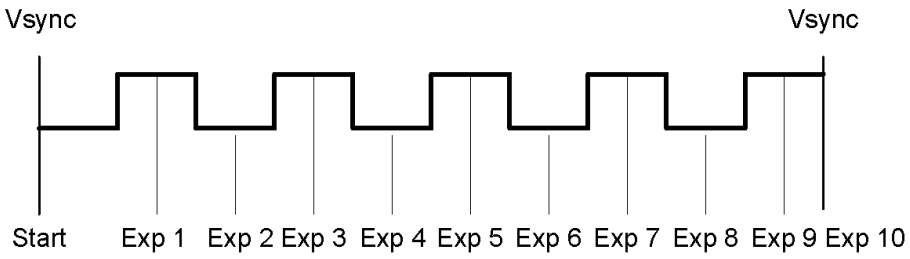

Figure 25. Timing of the camera exposures. All exposure starts when the VSync signal comes, and stops at different timing. Exposure 1, 2, …, and 10 use exposure time of 2.50, 4.17, 5.83, 7.50, 9.17, 10.83, 12.50, 14.17, 15.80, 16.67 ms.

is too short and the camera cannot capture the full projection period. The phase error for this exposure is very large (RMS 0.38 rad). Figure 26(c) shows one cross section of the phase error for the traditional FSP method after removing the unwrapped phase slope. Obviously, high-frequency periodical error components appear in the figure. Usually, the nonsinudoidal wavefrom results in periodical phase errors. The nonsinusoidal wavefrom is the result of the miss-capture of the camera. Because a DLP projector needs one full projection time to generate one grayscale image, any less exposure of the camera can result in an incorrect grayscale image.

For the DBP method, there are only two intensities (0 and 255). Our previous experiment result shown in Figure 20(a) indicates that when the projector is supplied with a pure green RGB = (0, 255, 0) image, the output signal has five periods during one projection cycle. We can use one period signal to represent the whole projection cycle signal. Thus, the exposure time could be any time.

Figure 26(b) shows the corresponding fringe image when the exposure time is set to be 2.50 ms. Compared with the fringe image shown in Figure 26(a), the fringe image for the

www.manaraa.com

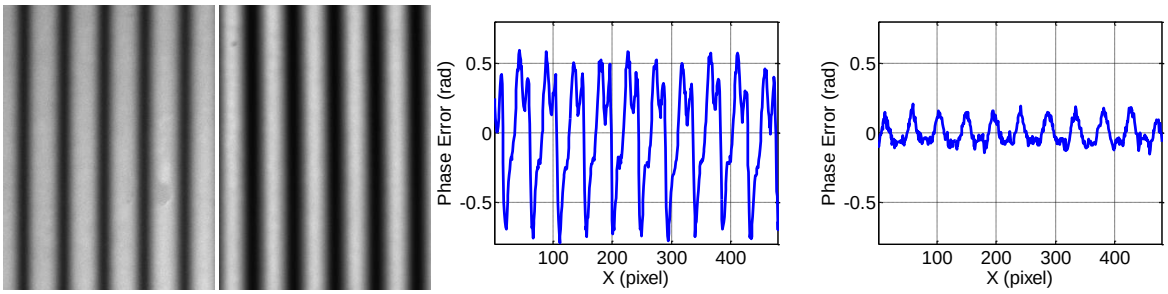

(a) (b) (c) (d)

Figure 26. Fringe images and phase errors if the exposure time is 2.50 ms. (a) Fringe image for the FSP method; (b) Fringe image for the DBP method; (c) One cross section of the phase error map for the FSP method (RMS: 0.38 rad); (d) One cross section of the phase error map for the DBP method (RMS: 0.08 rad).

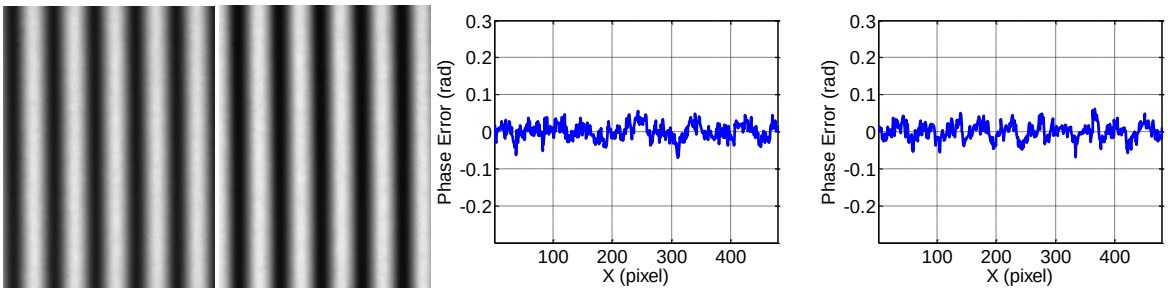

(a) (b) (c) (d)

Figure 27. Fringe images and phase errors if the exposure time is 16.67ms. (a) Fringe image for the FSP method; (b) Fringe image for the DBP method; (c) One cross section of the phase error map for the FSP method (RMS: 0.02 rad); (d) One cross section of the phase error map for the DBP method (RMS: 0.02 rad).

DBP method has a high quality. As a result, the phase error is much smaller (RMS 0.08 rad), as indicated in Figure 26(d).

When the exposure time is set to be 16.67 ms, the camera captures the full projection cycle, thus, whether for the FSP method or the DBP method, the camera cannot miss any

www.manaraa.com

information of one grayscale image projected by the projector. Figures 27(a)-(b) shows the fringe images captured by the FSP method and the DBP method, respectively, and both fringe images show sinusoidal patterns very clearly. Figures 27(c)-(d) show the one cross section of the phase error map for the FSP method and the DBP method, respectively, both phase errors appear to be random and smaller than those using the exposure time of 2.50 ms.

Figure 28 compares the phase error introduced by these two methods under different exposure times. Figure 28(a) shows the phase error when the exposure time is less than one full projection cycle. It clearly indicates that for the DBP method, the phase error does not change very much when the exposure time alters, while the FSP method does, especially when a very short exposure time is needed, and the phase error is very large. This experiment shows that if a very short (or arbitrary) exposure time is needed, the DBP method clearly outperforms the FSP method for 3-D shape measurement. This provides a potential way to develop a fast 3-D shape measurement technique.

Theoretically, the phase error is smaller when the exposure time increases due to the averaging effect. However, if the projection is not fully captured and the FSP method is used, the phase error is larger. When the exposure time is on full projection cycle, the FSP method should give better results if the gamma correction performs well. 6 different exposure times, 16.67, 25.00, 50.00, 58.33, 83.33, and 91.67 ms, are used for data acquisition. The camera starts its exposure when the VSync signal comes and stops at both full projection cycle (16.67, 50.00, 83.33 ms) and half projection cycle (25.00, 58.33, 91.67 ms). Figure 28(b) shows the phase error with six different exposure times. It shows that the phase error for the FSP method is similar to that for the DBP approach when the exposure time is on full projection cycle. However, when the camera does not capture the full projection, the phase

www.manaraa.com

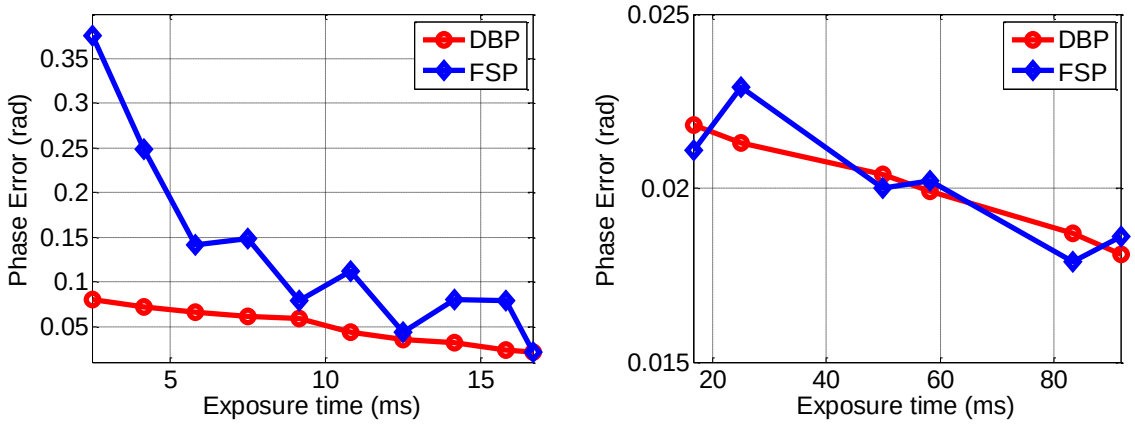

(a) (b)

Figure 28. Phase error for different exposure times.

error caused by the FSP method is larger than that is induced by the DBP approach.

To compare the 3-D shape measurement quality at various exposure times, 4 different exposure times (3.33, 6.67, 10.00, 16.67 ms) are used for data acquisition. Figure 29 shows 3-D reconstruction results of a complex sculpture for the DBP and the FSP methods with different exposure times. Figures 29(a)-(d) shows the results by the DBP methods with exposure times 3.33, 6.67, 10.00, and 16.67 ms, respectively. Figures 29(e)-(h) shows the results by the FSP methods with exposure times 3.33, 6.67, 10.00, and 16.67 ms, respectively. When the exposure time is set to be less than one projection cycle, the FSP method cannot get correct 3-D measurement, as shown in Figures 29(e)-(g). This is because the camera cannot capture the full projection period. However, for the DBP approach, it still provides good 3-D measurement, as shown in Figures 29(a)-(c). When the exposure time is on full projection cycle, both methods give good results, as shown in Figure 29(d) and Figure 29(h). The experimental results clearly indicate the DBP method outperforms the FSP method for 3-D shape measurement when the exposure time is less than one projection cycle.

www.manaraa.com

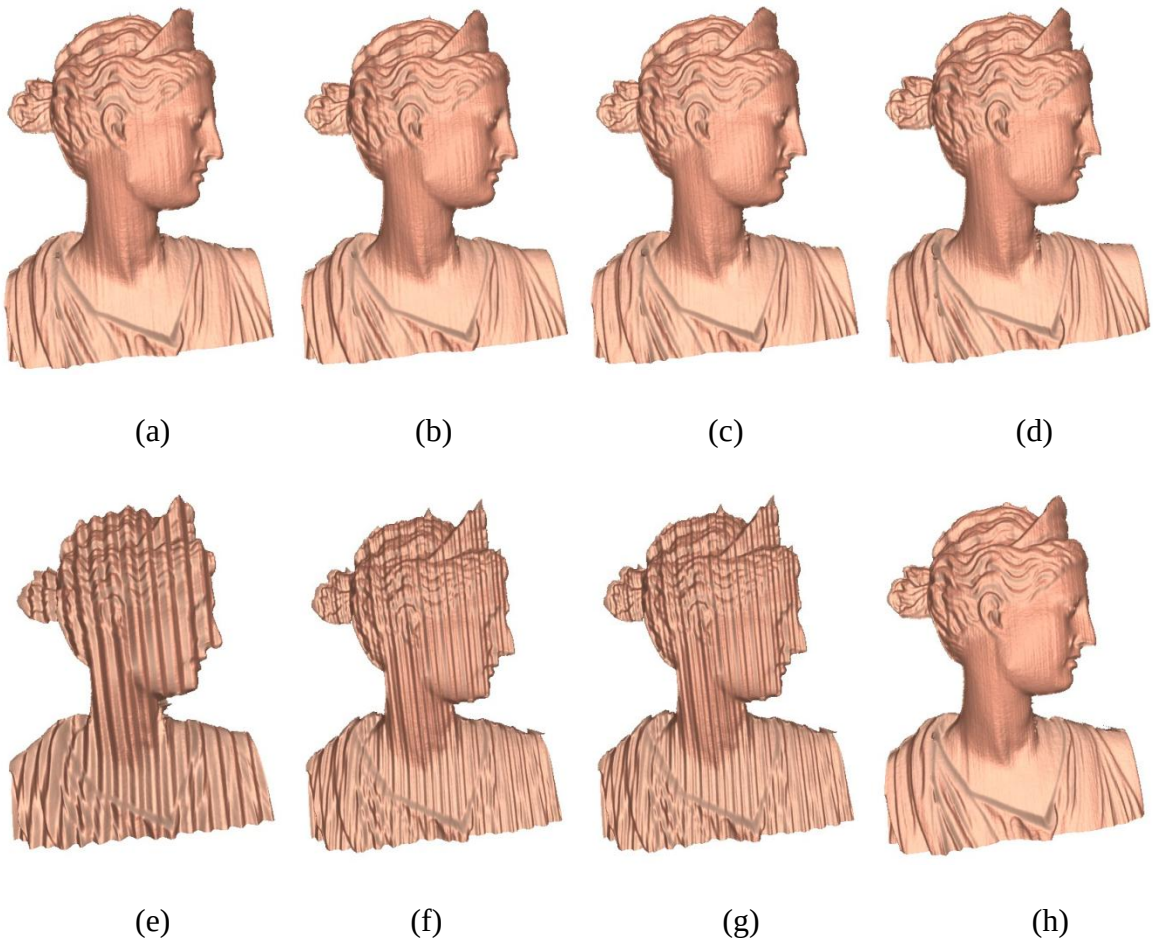

(a) (b) (c) (d)

(e) (f) (g) (h)

Figure 29. Measurement results of a complex sculpture for the DBP and the FSP methods with different exposures. (a)-(d) Results by the DBP method; (e)-(f) Results by the FSP method. From left to right, exposure times are: 3.33, 6.67, 10.00, and 16.67 ms.

5.4 Synchronization

The synchronization between the camera and the projection is usually complicated in real-time 3D shape measurement. Because the DLP projector generates the grayscale image by time modulation [21], the camera should capture the whole channel projection in order to acquire correct grayscale images. Therefore, if sinusoidal fringe patterns are supplied to a DLP projector, the synchronization between the projector and the camera plays an important

www.manaraa.com

role for high-quality 3-D shape measurement, especially when the exposure time is not long. The result in Figure 20(a) shows that when a pure green RGB = (0, 255, 0) image is sent to a projector, the output signal has five periods during one projection, and we can use any period signal to represent the whole projection signal. This indicates that the synchronization between the projector and the camera is not necessary for the DBP method.

To test how the synchronization between the projector and the camera influences the measurement, the external trigger of the camera is disabled, and the fringe images are captured at any time when the user starts it. The camera is always in focus. A uniform flat surface is imaged. For the FSP method, the projector is in focus, and the nonlinear gamma of the projector is applied. For the DBP method, the projector is properly defocused.

In this experiment, three specific exposure times are tested (3.33, 6.67, and 10.00 ms), while the starting timing is random. The exposure time is selected so that either one or several pulses of projection will be captured for the projection shown in Figure 20. For each exposure time, the software continuous runs with random delay between frames, and the camera captures 120 frames for future analysis.

Figures 30(a)-(c) show the phase errors for the DBP method when the exposure time is set to be 3.33 ms, 6.67 ms, and 10.00 ms, respectively. Figures 30(d)-(f) show the phase error for the FSP method when the exposure time is set to be 3.33 ms, 6.67 ms, and 10.00 ms, respectively. This result indicates that for the same exposure time, the phase error for the DBP method is much smaller than that for the FSP method.

Figure 31 shows some typical fringe images and corresponding cross sections for the DBP and the FSP methods when a very short exposure time of 0.5 ms is used. From Figures 31(a)-(d), it clearly shows that the fringe images only change the intensity over time for the

www.manaraa.com

DBP method, however, for the FSP method, these images vary both intensity and the profile, as shown in Figures 31(e)-(h). This experimental result indicates that the DBP method is less sensitive to the synchronization between the projector and the camera, and performs better than the FSP method when the camera is not precisely synchronized with the projector.

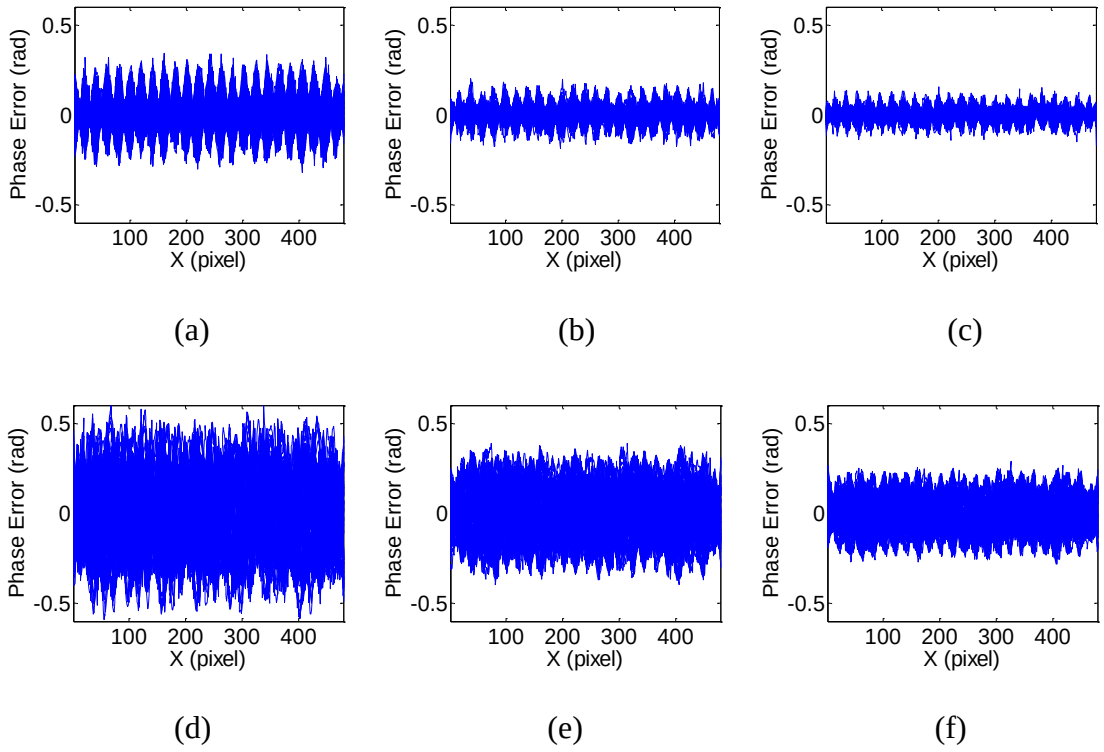

Figure 30. Phase error for different exposure times when the camera and the projector are not synchronized. (a) The DBP method with exposure time of 3.33 ms (RMS: 0.08 rad); (b) The DBP method with exposure time of 6.67 ms (RMS: 0.04 rad); (c) The DBP method with exposure time of 10.00 ms (RMS: 0.03 rad); (d) The FSP method with exposure time of 6.67 ms (RMS: 0.14 rad); (e) The FSP method with exposure time of 3.33 ms (RMS: 0.20 rad); (f) The FSP method with exposure time of 10.00 ms (RMS: 0.09 rad).

www.manaraa.com

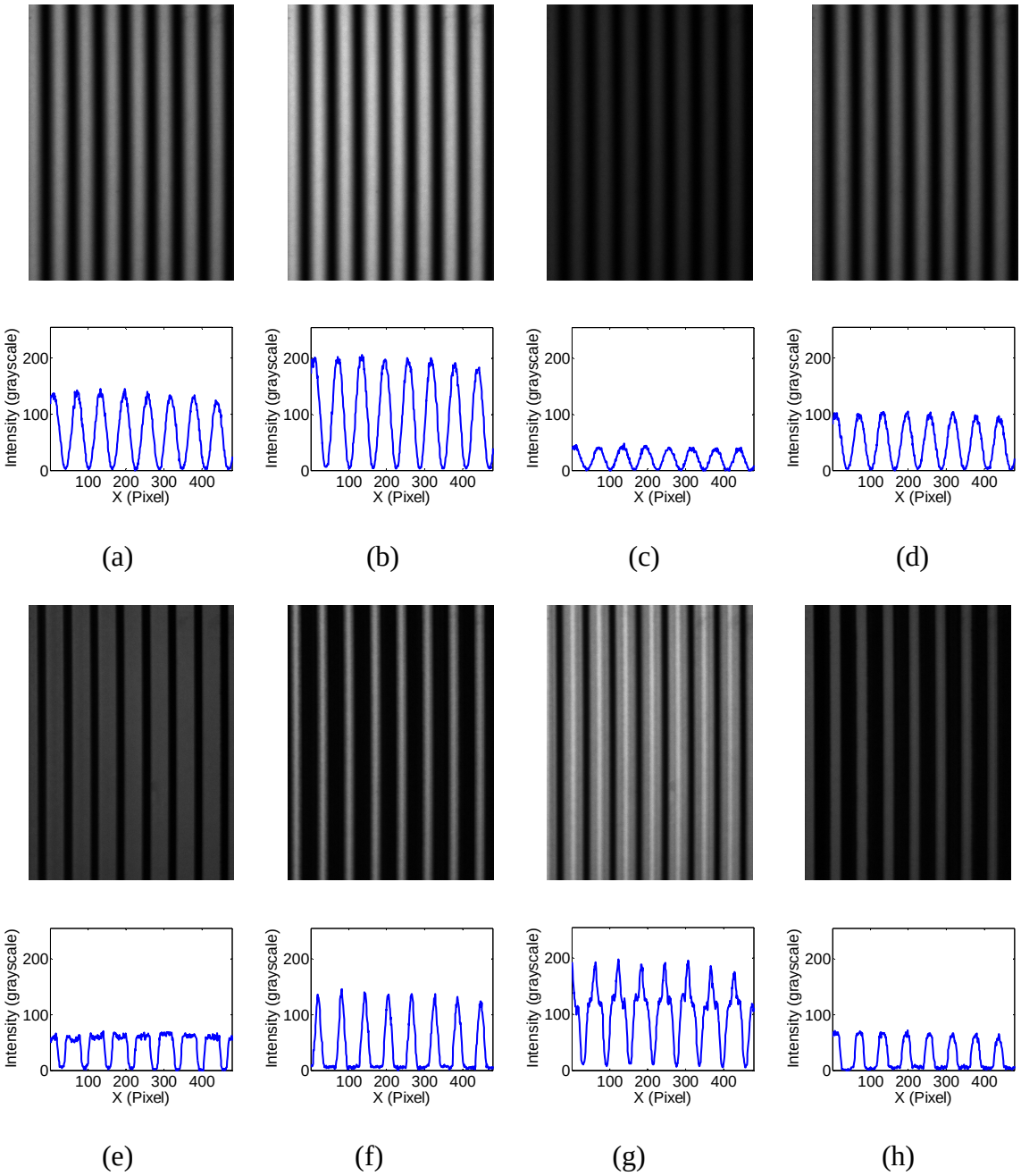

Figure 31. Examples for the 0.5 ms exposure time when the camera and the projector are not synchronized. (a)-(d) Examples of the DBP method, first row is the fringe patterns and second row is corresponding 100th cross section; (e)-(h) Examples of the FSP method, first row is the fringe patterns and second row is the corresponding 100th cross section.

www.manaraa.com

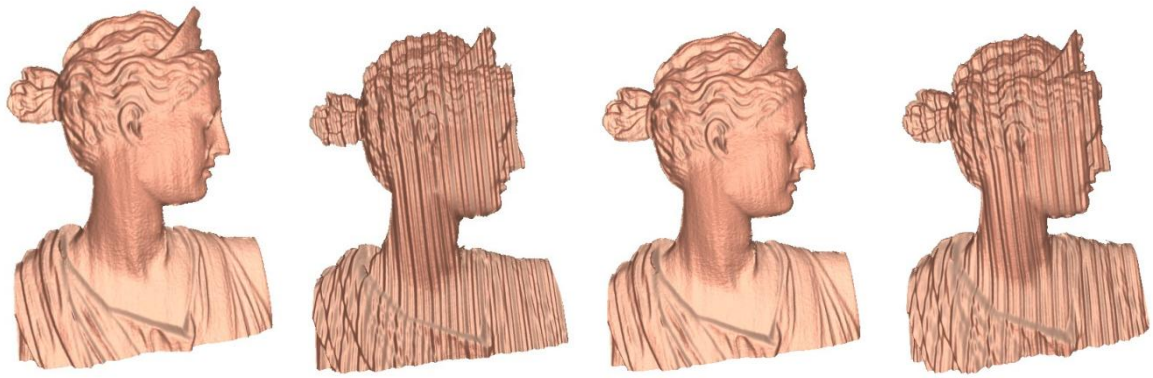

(a) (b) (c) (d)

Figure 32. Measurement results of a complex sculpture for the DBP and the FSP methods when the camera and the projector are not synchronized. (a) Result by the DBP method with an exposure time of 3.33 ms; (b) Result by the FSP method with an exposure time of 3.33 ms; (c) Result by the DBP method with an exposure time of 6.67 ms; (d) Result by the FSP method with an exposure time of 6.67 ms.

To compare the 3-D measurement quality when the projector and the camera are not synchronized, two specific exposure times are tested (3.33 ms and 6.67 ms), and the starting time is random. Figure 32 shows the measurement results with different exposure times. It clearly shows that for the DBP method, it can obtain a good 3-D shape, while for the FSP approach, it has a large measurement error without the synchronization between the projector and the camera.

5.5 Projector nonlinear gamma

The commercial video projector is usually a nonlinear device which is purposely designed to compensate for human vision. Therefore, to perform high-quality 3-D shape measurement using the FSP method, projector gamma calibration is usually mandatory. This

www.manaraa.com

nonlinear response will result in non-sinusoidal waveforms if no compensation is used. A variety of techniques have been studied including those to actively change the fringe to be projected [15, 16], and to passively compensate for the phase error [17-20]. These methods increase the complexity of the system development. Moreover, our experiments found that the projector nonlinear gamma changes overtimes, thus it need to be re-calibrated frequently for high quality measurement. While, for the DBP method, this should not be necessary because only two intensity values (0 and 255) are used, and the output light intensity does not change much when the input intensity is close to 0 or 255.

To test and compare how the projector nonlinear gamma influences the measurement, one exposure time of 16.67 ms is used to alleviate the problem caused by the synchronization between the projector and the camera. A uniform flat surface is imaged. The camera is always in focus during the process, and for the DBP method, the projector is properly defocused to a certain degree.

Figure 33(a) shows the one cross section of the phase error for the DBP method. The phase error is very small (RMS 0.02 rad) and appears to be random, which indicates that the phase error is not affected by the projector nonlinear gamma. Figure 33(b) shows the corresponding phase error for the FSP method without gamma correction. The phase error is significantly large (RMS 0.09 rad). Figure 33(c) is the phase error for the FSP method with applying gamma correction, and the phase error reduces to a very small number (RMS 0.02 rad). This is because for the FSP method, a full intensity range (0-255) is used, and the nonlinear effect of the projector plays an important role. However, for the DBP method, only two intensity values are used and the intensity of the output light does not change much.

www.manaraa.com

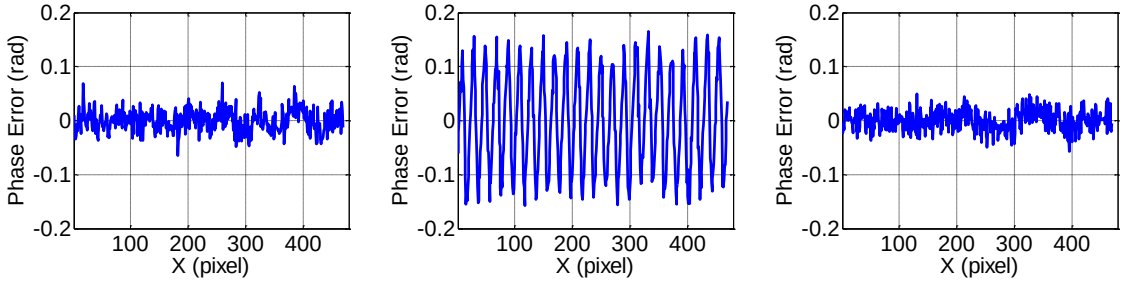

(a) (b) (c)

Figure 33. Phase errors (a) DBP method without projector gamma correction (RMS: 0.02 rad); (b) FSP method without projector gamma correction (RMS: 0.09 rad); (c) FSP method with projector gamma correction (RMS: 0.02 rad).

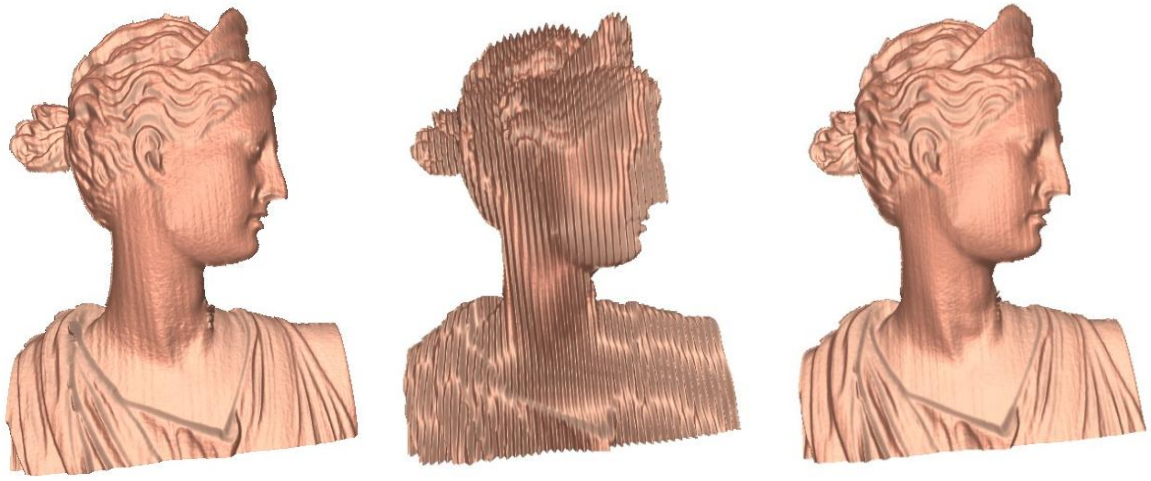

(a) (b) (c)

Figure 34. 3-D measuring results of sculptures. (a) DBP method without projector gamma correction; (b) FSP method without projector gamma correction; (c) FSP method with projector gamma correction.

To test and compare how the projector nonlinear gamma influences the 3-D shape measurement, the exposure time is set to be 16.67 ms to capture a full projection cycle, and the results are shown in Figure 34. It shows that if there is no projector gamma correction,

www.manaraa.com

the FSP method would cause a large measure error, as shown in Figure 34(b), while for the DBP approach, it still can get a high-quality reconstruction shape, as shown in Figure 34(a).

5.6 Discussion of results

In this thesis, we designed four experiments to analyze the phase error caused by the following effects: (a) defocusing degree, (2) exposure time, (3) synchronization between the projector and the camera, and (4) projector nonlinear gamma. The experiment results indicate that compared with the FSP approach, generating sinusoidal fringe patterns by the DBP method has the following major advantages:

(1) **No precise synchronization between the projector and the camera is necessary**. For the FSP method, the camera and the projector must be precisely synchronized for a high-quality 3-D shape measurement. On the contrast, for the DBP method, the sinusoidal fringe patterns are generated by defocusing binary patterns, and the synchronization is less important.

(2) **No gamma correction is required**. For the FSP method a full intensity range (0-255) is used, thus, projector gamma calibration is usually mandatory for a commercial digital video projector. On the contrast, the DBP method is not sensitive to the projector gamma because only two grayscale values are used.

(3) **It is very easy to generate sinusoidal fringe patterns**. This is because no complicated algorithms are necessary.

(4) **The measurement is less sensitive to the exposure time used**. Therefore, the defocused binary patterns method is advantageous for 3-D shape measurement using a commercial DLP projector.

www.manaraa.com

However, compared with the FSP method, the DBP is not trouble free. It still has some shortcomings:

(1) **More difficult to achieve high accuracy**. Because the sinusoidal patterns are not generated directly by the computer, the degree of defocusing affects the measurement. It seems to be impossible to generate perfect sinusoidal fringe patterns by defocusing. Because the defocusing cannot act like a perfect low-pass filter with sharp edge, it can only suppress the high-frequency harmonics, but not get rid of it. The sinusoidal fringe pattern by properly defocusing always has high-frequency harmonics, which will cause measurement errors. On the contrast, the FSP method uses an in-focused projector, and it does not have this problem because the measuring objects are placed near its focal plane.

(2) **Small depth measurement range**. For the DBP method, the projector must be properly defocused to generate ideal sinusoidal fringe patterns; otherwise, the nonsinusoidal waveform will cause large error. On the contrast, the FSP method is not very sensitive to this problem because the degree of defocusing will not affect the fringe profile.

Nevertheless, compared with its shortcomings, the DBP method can still be very useful when a commercial DLP projector is used for flexible 3-D shape measurement.

5.7 Conclusions

This chapter had a comparison study about the performance of the DBP method and the FSP approach by analyzing the phase errors introduced by the following issues: (1) degree of defocusing, (2) exposure time, (3) synchronization, and (4) projector nonlinear

www.manaraa.com

gamma. Some real 3D measurement results were presented to compare these two methods. Our experimental results demonstrated that: (1) when the projector is defocused to a certain degree, the phase error induced by the DBP method is very close to that caused by the FSP method, thus, it is possible to generate ideal sinusoidal fringe patterns by the DBP method; (2) when a very short exposure time is needed, the DBP method definitely outperforms the FSP method for 3-D shape measurement; (3) the DBP method is less sensitive to the synchronization between the projector and the camera; and (4) no gamma correction is required for the DBP method. Phase error analysis and real 3-D shape measurement data were also presented to demonstrate and compare these two methods.

www.manaraa.com

CHAPTER 6. CONCLUSION AND FUTURE WORK

This chapter summarizes this dissertation and provides some ideas of future work that might be important with this dissertation.

6.1 Summary

In this research, we have a comparison study about two different digital sinusoidal fringe generation techniques: DBP and FSP. We introduced the theory, and provided the simulation and experimental results to demonstrate the capabilities of generating sinusoidal fringe images by properly defocusing binary patterns.

We analyzed the phase errors for both methods caused by the following effects: (1) degree of defocusing, (2) exposure time, (3) synchronization, and (4) projector nonlinear gamma. Both simulation and experiments showed that for the DBP method, when the projector is defocused to a certain degree, the phase error induced by the DBP method is very close to that produced by the FSP approach.

The experiment results clearly show that for the DBP method, the phase error does not change significantly with the exposure time. This becomes important, especially, when a very short exposure time is needed, the DBP method definitely outperforms the FSP method for 3-D shape measurement. Thus, this DBP technique can be used to measure fast motion and the measurement speed can be greatly improved. Actually, some major pieces of work recently developed in our lab based on the DBP have verified that the projector defocusing technique can be used to reach the refreshing speed of a DLP projector: 120 HZ without significantly increasing the system cost [47], and achieve a 3-D shape measurement speed of 2000 kHZ with a simple and inexpensive DLP projector with a Fourier method [48].

www.manaraa.com

Generating sinusoidal fringe images by defocusing the binary patterns are less sensitive to the synchronization between the projector and the camera and the projector's nonlinear gamma. On the contrast, for a conventional method where the sinusoidal fringe images are generated by the computer and projected by the focused projector, all these factors must be well controlled to ensure high-quality measurement.

However, the DBP method is not trouble free. One of the major issues is that it seems to be impossible to generate ideal sinusoidal fringe patterns by defocusing, because the seemingly sinusoidal fringe pattern actually has high-frequency harmonics, which introduces measurement error. Another problem involves the depth range. Measurement range by using this technique is smaller than the conventional fringe generation methods. This is because the defocusing degree should be properly controlled, and cannot be too little or too much for high-quality measurement. We are currently seeking hardware and software approaches to solve these problems without sacrificing the merits of the proposed technique.

The proposed technique to generate sinusoidal fringe patterns has significantly simplified the development of 3-D shape measurement system, and provides a potential way to develop high-speed imaging. Therefore, it has the potential to replace the conventional fringe generation technique for the 3-D shape measurement system based on fringe analysis and phase-shifting methods.

6.2 Future work

In this dissertation, we have studied a recently developed new sinusoidal fringe generation technique that generates sinusoidal fringe patterns with a DLP by using the DBP method instead of the traditional FSP method. This technique has significantly simplified the

www.manaraa.com

3-D shape measurement system development since the projector nonlinearity does not bring any problems into the imaging system. This may lead to some breakthroughs in the field of high-speed 3-D shape measurement. However, there are a number of avenues to explore in order to advance this technique. The future work tasks fall into three areas:

(1) **Dealing with high-frequency harmonics phase errors**. Essentially, defocusing is to suppress the high-frequency harmonic components of the binary structured patterns. However, some experiments developed based on the DBP technique found that the seemingly sinusoidal fringe patterns are still composed of high-frequency harmonics [47,48], and the nonsinusoidality of the fringe patterns causes phase errors. Therefore, to realize high-quality 3-D shape measurement, the phase errors introduced by the harmonics need to be reduced by either hardware or software means.

(2) **Increasing the measurement range**. Given the results in Section 5.2, we notice that the degree of defocusing is controlled by manually adjusting the focal length of the projector. The phase error induced by the DBP method is very similar with that caused by the FSP method. Defocusing either too little or too much will influence the measurement. Therefore, the high-quality fringe patterns can be generated within a small depth range. This means that the high-quality measurement can be obtained within a relatively small depth range. Future research needs to be conducted to increase the depth range.

(3) **Calibrating defocused projector**. All the existing techniques assume the projector to be in focus, which is not the case for our system. The calibration

www.manaraa.com

involving a defocused projector will be more complicated. Currently, we are seeking a new method to accurately calibrate a defocused projector.

www.manaraa.com

ACKNOWLEDGEMENTS

I would like to take this opportunity to express my gratitude and thanks to those who helped me with various aspects of conducting research and writing this thesis. Without their support, this would not be possible.

First and foremost, I would like to thank my advisor Dr. Zhang. His inspiring advice guides me throughout my research and study during the past one and a half years. His kindness makes my work a pleasant experience. His support helped me with the challenges that arose during my research. I would like to express my respect and cordial thanks to him.

Next, I would like to express my sincere gratitude to my committee member Dr. James Oliver, whose kindness helped me get a scholarship this fall semester, which gives me lots of confidence in my studies and research. Further, I would like to thank committee members Dr. Eliot Winer and Dr. Lie Tang, who are doing a favor for me by being on my committee.

Next, I thank Yuanzheng Gong, Ying Xu, and Yajun Wang in the 3D Machine Vision Laboratory, for their help to me.

Last but not least, I owe the success of this thesis to my family for their love and support. I would not be here today without their continued love and support.

www.manaraa.com

REFERENCES

[1] Gorthi, S. S. and Rastogi, P. (2010). Fringe projection techniques: whither we are?. *Optics and Laser in Engineering*, 48(2), 133-140.

[2] Wang, Z., Nguyen, D. A., and Barnes, J. C. (2010). Some practical considerations in fringe projection profilometry. *Optics and Laser in Engineering*, 48(2), 218-225.

[3] Zhang, S. (2010). Recent progresses on real-time 3D shape measurement using digital fringe projection techniques. *Optics and Laser in Engineering*, 48(2), 149-158.

[4] Klette, R., Schluns, K. and Koschan, A. (1998). *Computer vision: three-dimensional data from images*. New York: Springer.

[5] Ribo, M. and Brandner, M. (2005). State of the art on vision-based structured light systems for 3-D measurements. *IEEE International Workshop on Robotic Sensors: Robotic and Sensor Environments*, Sep., 2-7.

[6] Zhang, S. and Huang, P. S. (2006). High-resolution, real-time three-dimensional shape measurement. *Optical Engineering*, 45(12), 123601.

[7] Chen, S., Li, Y., and Zhang, J. (2008). Vision processing for realtime 3-D data acquisition based on coded structured light. *IEEE Transactions on Image Processing*, 17(2), 167-176.

[8] Chen, X., Xi, J., Jiang, T. and Jin, Y. (2010). Research and development of an accurate 3D shape measurement system based on fringe projection: Model analysis and performance evaluation. *Precision Engineering*, 32(3), 215-221.

[9] Namboodiri, V. P. and Chaudhuri, S. (2007). On defocus, diffusion and depth estimation. *Pattern Recognition Letters*, 28(3), 311-319.

www.manaraa.com

[10] Hinojosa, C., Serrano-Heredia, A., and Ibarra, J. G. (1998). Recovery of three-dimensional shapes by using defocused structured light. *Optics & Laser Technology*, 30(5), 281-290.

[11] Wang, Y., Gupta, M., Zhang, S., Gu, X., Samaras, D., et al. (2008). High resolution tracking of non-rigid 3D motion of densely sampled data using harmonic maps. *International Journal of Computer Vision*, 76(3), 283-300.

[12] Chen, L., and Chang, Y. (2008). High accuracy confocal full-field 3-D surface profilometry for microlenses using a digital fringe projection strategy. *Key Engineering Materials*. 364-366, 113-116.

[13] Radiohead (2008), Radiohead: house of cards. Online: http://www.youtube.com/watch?v=8nTFjVm9sTQ.

[14] Zhou, G., Li, Z., Wang, C., and Shi, Y. (2009). A novel method for human expression rapid reconstruction. *Tsinghua Science & Technology*, 14(S1), 62-65.

[15] Kakunai, S., Sakamoto, T. and Iwata, K. (1999). Profile measurement taken with liquid-crystal grating. *Applied Optics*, 38(13), 2824-2828.

[16] Huang, P. S., Zhang, C. and Chiang, F. P. (2003). High-speed 3-D shape measurement based on digital fringe projection. *Optical Engineering*, 42(1), 163-168.

[17] Zhang, S. and Huang, P. S. (2007). Phase error compensation for a 3-D shape measurement system based on the phase shifting method. *Optical Engineering*, 46(6), 063601.

[18] Zhang, S. and Yau, S. T. (2007). Generic nonsinusoidal phase error correction for three-dimensional shape measurement using a digital video projector. *Applied Optics*, 46(1), 36-43.

www.manaraa.com

[19] Gao, H., He, H., and Chen, M. (2004). Gamma correction for digital fringe projection profilometry. *Applied Optics*, 43(14), 2906-2914.

[20] Pan, B., Kemao, Q., Huang, L. and Asundi, A. (2009). Phase error analysis and compensation for nonsinusoidal waveforms in phase-shifting digital fringe projection profilometry. *Optics Letters*, 34(4), 416-418.

[21] Hornbeck, L. J. (1997). Digital light processing for high-brightness, high-resolution application. *Processing of SPIE*, 3013, 27-40.

[22] Höfling, R. (2004). High-speed 3D imaging by DMD technology. *Processing of SPIE*, 5303, 188-194.

[23] Höfling, R. and Ahl, E. (2004). ALP: Universal DMD controller for metrology and testing. *Processings of SPIE*, 5289B, *322*-329.

[24] Lei, S and Zhang, S. (2009). Flexible 3-D shape measurement using projector defocusing. *Optics Letters*, 34(20), 3080-3082.

[25] Backer, M. J., Xi, J., Chicharo, J., and Li, E. (2005). A contrast between DLP and LCD digital projection technology for triangulation based optical profilometers. *Processings of SPIE*, 6000, 60000G.

[26] Gong, Y. and Zhang, S. (2010). Ultrafast 3-D shape measurement with an off-the-shelf DLP projector. Optical Express,18(19), 19743-19754.

[27] Quan, C., Jay, C. J., Shang, H. M., and Bryanston-Cross, P. J. (1995). Contour measurement by fiber optics fringe projection and Fourier transform analysis. *Optics Communications*, 118(5-6), 479-483.

www.manaraa.com

[28] Pawlowski, M. E., Kujawinska, M., and Wgiel, M. G. (2002). Shape and motion measurement of time-varying three-dimensional objects based on spatiotemporal fringe-pattern analysis. *Optical Engineering*, 41(2), 450-459.

[29] Huang, Y. H., Quan, C., Jay, C. J. and Chen, L. J. (2005). Shape measurement by the use of digital image correlation. *Optical Engineering*, 44(8), 087011.

[30] Takeda, M. (2010). Measurement of extreme physical phenomena by Fourier fringe analysis. *AIP Conference Proceedings*, 1236(1), 445-448.

[31] Li, Y., Jin, K., Jin, H. and Wang, H. (2010). High-resolution, high-speed 3D measurement based on absolute phase measurement. *AIP Conference Preceedings*, 1236(1), 389-394.

[32] Lei, S. and Zhang, S. (2010). Digital sinusoidal fringe pattern generation: Defocusing binary patterns VS focusing sinusoidal patterns. *Optics and LaserEngineering*, 48(5), 561-569.

[33] Ghiglia, D. C. and Pritt, M. D. (1998). *Two-dimensional phase unwrapping: theory, algorithms, and software*. New York: Wiley.

[34] Malacara, D. (2007). *Optical shop testing*. New York: John Wiley & Sons.

[35] Subbarao, M., Yuan, T., and Tyan, J. K. (1997). Integration of defocus and focus analysis with stereo for 3D shape recovery. *Proceedings of SPIE*, 3204, 11-23.

[36] Goodman, J. W. (2005). *Introduction to Fourier optics*. Englewood: Roberts & Co.

[37] Wikipedia, http://en.wikipedia.org/wiki/Fourier_optics.

[38] Yoshizawa, T. (2009). *Handbook of optical metrology: principles and application*. Boca Roton: CRC Press.

www.manaraa.com

[39] Rossmann, K. (1969). Point spread-function, line spread-function, and modulation transfer function, tools for the study of imaging systems. *Radiology*, 93(2), 257-272.

[40] Wikipedia, http://en.wikipedia.org/wiki/Point_spread_function.

[41] Wikipedia, http://en.wikipedia.org/wiki/Airy_disc.

[42] Chaudhuri, S. and Rajagopalan, A. N. (1999). *Depth from defocus: a real aperture imaging approach*. New York: Springer.

[43] Pentland, A. P. (1987). A new sense for depth of filed. *IEEE transactions on Pattern Analysis and Machine Intelligence*, 9(4), 523-531.

[44] Mathworld: http://mathworld.wolfram.com/Convolution.html.

[45] Ragulskies, M., Aleksa, A. and Maskeliunas, R. (2009). Contrast enhancement of time-averaged fringes based on moving average mapping function. *Optics and Laser in Engineering*, 47(7-8), 768-773.

[46] Hutchison, D. C. (2008). Introducing brilliantColor™ technology, *Technical report*, Texas Instrument. Online: http://www.scribd.com/doc/6695597/Introducing-Brilliant-Color-Technology

[47] Gong, Y. and Zhang, S. (2010). Improving 4-D shape measurement by using projector defocusing. *Proceedings of SPIE*, 7790, 77901A.

[48] Li, J. and Zhang, S. (2010). Generating sinusoidal fringe by defocusing: potentials for unprecedentedly high-speed 3-D shape measurement using a DLP projector. *Proceedings of SPIE*, 7790, 77900B.

www.manaraa.com